ETH zürich

A stellar census of the nearby, young 32 Orionis group

Author(s):
Bell, Cameron P.M.; Murphy, Simon J.; Mamajek, Eric E.

A stellar census of the nearby, young 32 Orionis group

Cameron P. M. Bell,[1,2]★ Simon J. Murphy[3] and Eric E. Mamajek[4,5]

[1]*Institute for Astronomy, ETH Zürich, Wolfgang-Pauli-Strasse 27, CH-8093 Zürich, Switzerland*
[2]*Leibniz Institute for Astrophysics Potsdam (AIP), An der Sternwarte 16, D-14482 Potsdam, Germany*
[3]*School of Physical, Environmental and Mathematical Sciences, University of New South Wales, Northcott Drive, Canberra, ACT 2600, Australia*
[4]*Department of Physics and Astronomy, University of Rochester, Rochester, NY 14627, USA*
[5]*Jet Propulsion Laboratory, California Institute of Technology, 4800 Oak Grove Drive, Pasadena, CA 91109, USA*

ABSTRACT

The 32 Orionis group was discovered almost a decade ago and despite the fact that it represents the first northern, young (age ~ 25 Myr) stellar aggregate within 100 pc of the Sun ($d \simeq 93$ pc), a comprehensive survey for members and detailed characterization of the group has yet to be performed. We present the first large-scale spectroscopic survey for new (predominantly M type) members of the group after combining kinematic and photometric data to select candidates with Galactic space motion and positions in colour–magnitude space consistent with membership. We identify 30 new members, increasing the number of known 32 Ori group members by a factor of 3 and bringing the total number of identified members to 46, spanning spectral types B5 to L1. We also identify the lithium depletion boundary (LDB) of the group, i.e. the luminosity at which lithium remains unburnt in a coeval population. We estimate the age of the 32 Ori group independently using both isochronal fitting and LDB analyses and find it is essentially coeval with the β Pictoris moving group, with an age of 24 ± 4 Myr. Finally, we have also searched for circumstellar disc hosts utilizing the All*WISE* catalogue. Although we find no evidence for warm, dusty discs, we identify several stars with excess emission in the *WISE W*4 band at 22 μm. Based on the limited number of *W*4 detections, we estimate a debris disc fraction of 32^{+12}_{-8} per cent for the 32 Ori group.

Key words: stars: fundamental parameters – stars: kinematics and dynamics – stars: pre-main-sequence – open clusters and associations: general – solar neighbourhood.

1 INTRODUCTION

The region surrounding the Sun out to a distance of $\sim$100 pc is often referred to as the 'Local Bubble' on account of the relatively low density of the interstellar medium and the accompanying lack of active star-forming regions. Hence, the discovery just over three decades ago of young, seemingly isolated T-Tauri stars in close proximity to the Sun was a watershed moment and precipitated a massive observational effort to characterize the young population of the Local Bubble (see e.g. Rucinski & Krautter 1983; de la Reza et al. 1989; Gregorio-Hetem et al. 1992; Webb et al. 1999). Our understanding of this young population has increased dramatically since these early discoveries with the advent of all-sky astrometric and X-ray/UV surveys. Not only have hundreds of additional young stars been identified and spectroscopically characterized within this region, but more importantly, it has been demonstrated that many of these stars comprise kinematically distinct, yet spatially dispersed groups within which the members share a common motion through space (see e.g. Torres et al. 2000; Zuckerman & Webb 2000). To

date, approximately one dozen such groups have been identified within 100 pc with ages ranging from $\sim$10 to 200 Myr (see reviews by Zuckerman & Song 2004; Torres et al. 2008; Mamajek 2016).

The study of nearby young moving groups plays an important role in constraining theories of star and planet formation. Given their youth and proximity to Earth, these moving groups provide the best available samples to investigate the early evolution of low- to intermediate-mass stars (see e.g. Mamajek & Bell 2014). In addition to their obvious importance regarding stellar astrophysics and in particular the pre-main-sequence (pre-MS) phase, these groups also represent the most readily accessible targets for direct imaging (and other measurements/studies) of dusty circumstellar discs; especially during the epoch of terrestrial planet formation (see e.g. Canup 2004). Finally, constituent members of these groups are ideal candidates for the discovery and characterization of young, substellar objects and, of course, extrasolar planets (see e.g. Lagrange et al. 2010).

1.1 The 32 Orionis group

Unlike other nearby young moving groups and associations, the 32 Ori group has received little attention in the literature despite
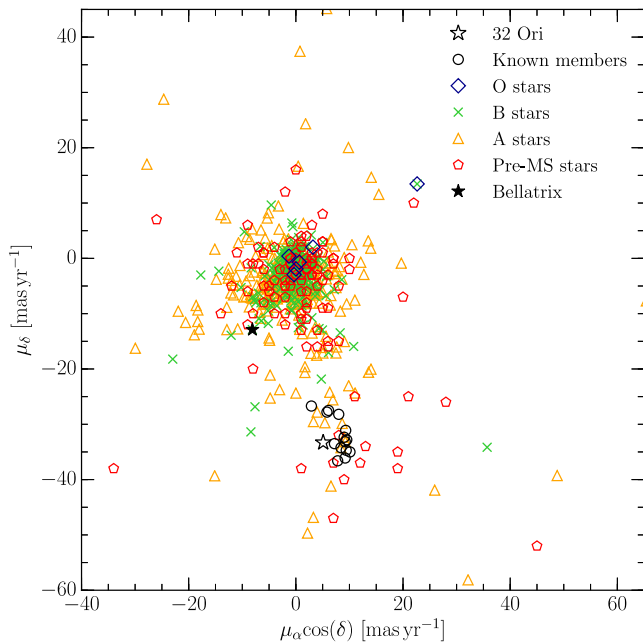
★ E-mail: cbell@aip.de

Figure 1. Proper motions of stars within 10° of 32 Ori. Proper motions for the O-, B- and A-type stars (including 32 Ori and Bellatrix; see the 'Introduction') are taken from the revised *Hipparcos* reduction, whereas the pre-MS stars are from the catalogue of Ducourant et al. (2005). Those for the known members are compiled from a combination of the revised *Hipparcos* reduction, PPMXL and UCAC4 (see Table 1). The majority of stars have small proper motions and are associated with the more distant Orion OB1 and λ Orionis associations at ∼400 pc; however, there is an appreciable concentration of stars with proper motions similar to that of 32 Ori.

its discovery almost a decade ago, and as such its stellar population remains poorly characterized. Mamajek (2007) was the first to present evidence of a young stellar aggregate (age ∼25 Myr; designated Mamajek 3) associated with the B5IV+B7V binary 32 Ori based on a concentration of comoving stars in a proper motion diagram. Fig. 1 shows the proper motions of stars within 10° of 32 Ori, for which the O-, B-, and A-type stars (including Bellatrix and 32 Ori itself) are taken from the revised *Hipparcos* reduction of van Leeuwen (2007). Also plotted are pre-MS stars from the catalogue of Ducourant et al. (2005) and the 15 known stellar members of the 32 Ori group, compiled from a combination of *Hipparcos*, PPMXL (Röser, Demleitner & Schilbach 2010) and the Fourth US Naval Observatory CCD Astrograph Catalog (UCAC4; Zacharias et al. 2013).

While the majority of stars in Fig. 1 have small proper motions ($\lesssim$10 mas yr^{-1}) and are associated with the more distant (∼400 pc) Orion OB1 and λ Orionis associations, there is a clear concentration of stars in proper motion space in the vicinity of 32 Ori. Within this concentration, there are three A-type stars with *Hipparcos* entries (HR 1807 [HIP 25453], HD 36823 [HIP 26161] and HD 35714 [HIP 25483]) that are all approximately co-distant with 32 Ori and that together provide a weighted mean group distance of 92.9 ± 2.3 pc. Also appearing to be comoving with 32 Ori are several X-ray bright late-type stars discovered by the *ROSAT* All-Sky Survey (Voges et al. 1999). Spectroscopic follow-up of a subset of these was performed by Alcalá et al. (1996, 2000) who measured strong lithium (Li) absorption in addition to deriving radial velocities that are consistent with that of 32 Ori (18.6 ± 1.2 km s^{-1}; Barbier-Brossat & Figon 2000).

To date, a total of 15 stars have been identified as members of the 32 Ori group, in addition to a potential planetary-mass object (Burgasser et al. 2016; see Section 4.2). The stellar members have been compiled primarily by Mamajek and collaborators (Mamajek 2007; Shvonski et al. 2016) – but see also additions by Mace et al. (2009) and Franciosini & Sacco (2011) – over the last decade, with new members being assigned on the basis of various diagnostics including common proper motion, radial velocities, Hα emission and Li absorption. Note that the recent study of Bell, Mamajek & Naylor (2015) only included 14 stellar members of the group, having neglected HD 36823. This star has been shown to be a wide, common proper motion companion to HD 35714 (Shaya & Olling 2011), and so we include it here in our list of known group members. Table 1 provides positions, spectral types, proper motions and radial velocities for the 15 known stellar members of the 32 Ori group, while Table 2 lists the mean group position, parallax, proper motion, radial velocity and Galactic *UVW* velocity. The spectral types listed in Table 1 for all stars other than 32 Ori and HR 1807 have been determined through visual comparison of flux-calibrated spectra acquired over the past decade against a dense grid of MK spectral standards (see Shvonski et al. 2016). Fig. 2 depicts the *UVW* velocity of the 32 Ori group relative to other young groups and associations within 100 pc. Velocities for the other young groups were taken from the recent compilation of Mamajek (2016), except for Argus that is from Gagné et al. (2014). Interestingly, not only does the 32 Ori group appear very close in velocity to the β Pictoris moving group (BPMG) in all three *UVW* planes, but the two groups also have very similar ages (see Bell et al. 2015 and the discussion in Section 5).

Two of the 15 stars listed in Table 1 (TYC 112-1486-1 and TYC 112-917-1) have previously been classified as members of the BPMG by Elliott et al. (2014). Using the Bayesian Analysis for Nearby Young AssociatioNs (BANYAN) II web tool (Malo et al. 2013; Gagné et al. 2014), we calculate that both stars have BPMG membership probabilities of $\lesssim$2 per cent, whereas the probabilities that they are associated with the young field are much higher ($\simeq$90 per cent). Furthermore, their kinematic distances (see Section 2.1 for details) are ∼80 pc for BPMG (adopting the *UVW* velocity from Mamajek 2016). Hence, if both stars are genuine BPMG members, they would be two of the most distant members of the group, at approximately twice the ∼40 pc median distance of the 'classic' membership list of Zuckerman & Song (2004, see also Mamajek & Bell 2014). Based on this evidence, we retain both TYC 112-1486-1 and TYC 112-917-1 as 32 Ori group members for this study and include them in our determination of the mean group properties listed in Table 2.

Shvonski et al. (2016) describes a *Spitzer* IRAC and MIPS survey of the 32 Ori group that was performed during 2007/08, covering all bandpasses from 3.6 to 70 µm (see also Shvonski et al. 2010). In this study, the authors combined the *Spitzer* photometry with optical and near-infrared (IR) data to quantify excess emission arising from circumstellar material. Shvonski et al. (2016) report that 4/14 members exhibit excess 24 µm emission: HR 1807 ($f_{24} = 88.45 \pm 0.36$ mJy), HD 35499 ($f_{24} = 8.45 \pm 0.10$ mJy), HD 36338 ($f_{24} = 14.79 \pm 0.15$ mJy) and TYC 112-1486-1 ($f_{24} = 3.87 \pm 0.09$ mJy). HR 1807 also exhibits a 70 µm excess ($f_{70} = 91.0 \pm 4.2$ mJy). Note that the quoted fluxes represent total fluxes and correspond to excess emission more than 4σ above typical photospheric levels. Modelling the excess emission, Shvonski et al. (2016) determined that the dust temperatures associated with these debris disc candidates were $\lesssim$200 K.

Table 1. Properties of the 15 known stellar members of the 32 Ori group.

Name	α (J2000.0) (hh mm ss.ss)	δ (J2000.0) (hh mm ss.s)	SpT	Ref.	$\mu_\alpha\cos(\delta)$ (mas yr^{-1})	μ_δ (mas yr^{-1})	Ref.	RV (km s^{-1})	Ref.
32 Ori	05 30 47.05	+05 56 53.3	B5IV+B7V	1	5.10 ± 0.67	−33.30 ± 0.35	2	18.6 ± 1.2	3
HR 1807	05 26 38.83	+06 52 07.2	B9.5V	4	9.22 ± 0.56	−33.15 ± 0.31	2	13.1 ± 2.5	5
HD 35714	05 26 59.99	+07 10 13.0	A3	6	9.34 ± 0.04	−32.97 ± 0.03	7	35.4 ± 1.0	8
HD 36823	05 34 38.42	+06 07 36.7	A7.5	9	9.07 ± 0.05	−31.67 ± 0.02	7	–	–
HD 35499	05 25 14.56	+04 11 48.2	F4	6	8.29 ± 0.54	−29.02 ± 0.56	7	–	–
HD 36338	05 31 15.70	+05 39 46.4	F4.5	6	9.48 ± 0.48	−32.76 ± 0.54	7	–	–
HD 35695	05 26 52.03	+06 28 22.7	F9	6	9.20 ± 0.80	−36.10 ± 1.20	10	–	–
HD 245567	05 37 18.43	+13 34 52.5	G5	6	7.20 ± 0.90	−33.50 ± 0.80	10	14.9 ± 0.8	11
HD 245059	05 34 34.91	+10 07 06.4	G7	6	10.10 ± 1.30	−35.00 ± 1.20	10	19.8 ± 1.0	12
TYC 112-1486-1	05 20 31.82	+06 16 11.6	K3	6	9.50 ± 1.80	−32.80 ± 2.10	10	18.5 ± 0.2	13
TYC 112-917-1	05 20 00.29	+06 13 03.7	K4	6	9.40 ± 1.90	−34.70 ± 2.10	10	18.8 ± 0.1	13
2MASS J05234246+0651581	05 23 42.46	+06 51 58.2	K6.5	6	7.80 ± 2.30	−36.60 ± 2.80	10	18.4 ± 1.0	12
V1874 Ori[a]	05 29 19.00	+12 09 29.6	K6.5	6	2.90 ± 2.10	−26.70 ± 3.00	10	18.4 ± 0.3	14
2MASS J05253253+0625336	05 25 32.54	+06 25 33.7	M3	6	8.00 ± 5.80	−28.20 ± 6.10	10	–	–
2MASS J05194398+0535021	05 19 43.98	+05 35 02.2	M3	6	5.80 ± 4.00	−27.80 ± 4.00	15	–	–

[a]Double-lined spectroscopic binary. The quoted radial velocity is the centre-of-mass velocity.
References for spectral types, proper motions and radial velocities: (1) Edwards (1976), (2) van Leeuwen (2007), (3) Barbier-Brossat & Figon (2000), (4) Abt & Morrell (1995), (5) Bobylev, Goncharov & Bajkova (2006), (6) Shvonski et al. (2016), (7) Gaia Collaboration et al. (2016), (8) Gontcharov (2006), (9) Mark Pecaut (private communication), (10) Zacharias et al. (2013), (11) White, Gabor & Hillenbrand (2007), (12) Alcalá et al. (2000), (13) Elliott et al. (2014), (14) Mace et al. (2009), (15) Röser et al. (2010).

Table 2. Mean properties of the 32 Ori group (Mamajek 3).

α (J2000.0) (hh mm ss.ss)	δ (J2000.0) (hh mm ss.s)	π^a (mas)	$\mu_\alpha\cos(\delta)$ (mas yr^{-1})	μ_δ (mas yr^{-1})	RV^b (km s^{-1})	U (km s^{-1})	V (km s^{-1})	W (km s^{-1})
05 27 16.32	+06 40 37.2	10.49 ± 0.22	8.6 ± 0.5	−32.6 ± 0.5	18.6 ± 0.2	−11.8 ± 0.3	−18.9 ± 0.3	−8.9 ± 0.3

[a]Calculated using the seven stars with trigonometric parallax measurements from the revised *Hipparcos* reduction and *Gaia* DR1 (32 Ori, HR 1807, HD 35714, HD 36823, HD 35499, HD 36338 and TYC 112-1486-1).
[b]The mean group radial velocity does not include the velocities of HR 1807 and HD 35714. Unlike 32 Ori, for which the value in Table 1 represents the mean of 39 observations, single-epoch measurements of rapidly-rotating early-type stars are notoriously unreliable.
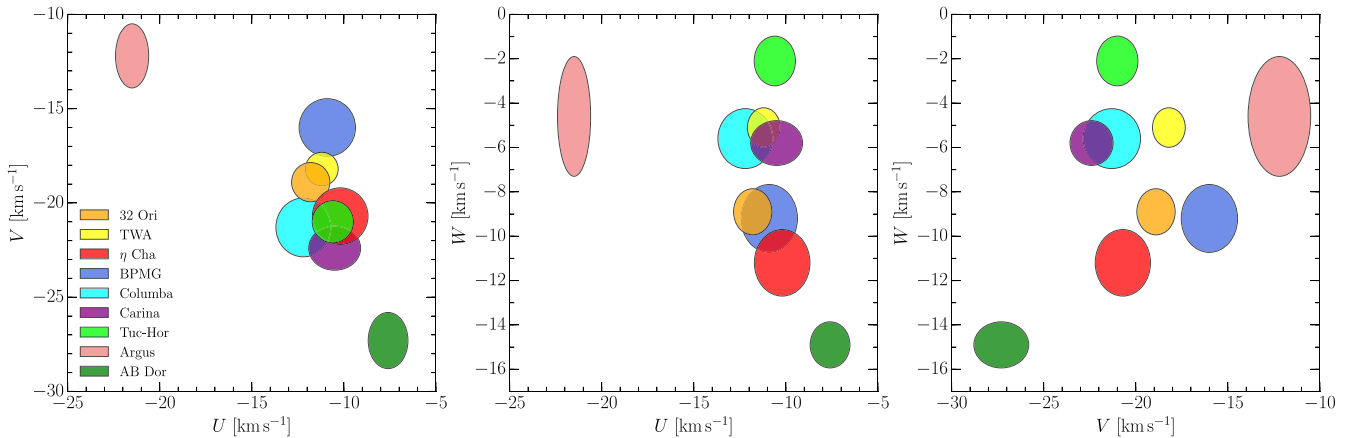

Figure 2. Galactic *UVW* velocity of the 32 Ori group relative to other young groups and associations within 100 pc. Ellipses represent the observed velocity dispersion of each group, i.e. the uncertainties in the mean velocities (σ_U, σ_V, σ_W) added in quadrature with the intrinsic one-dimensional velocity dispersion (typically $\lesssim$1.5 km s^{-1}). In all three planes, the 32 Ori group lies close in velocity space to the β Pictoris moving group (BPMG).

Recently, Bouy & Alves (2015) argued that the 32 Ori group should in fact be termed the 'Bellatrix cluster' on the basis that the sky position, distance (77^{+4}_{-3} pc; van Leeuwen 2007) and age (20^{+2}_{-4} Myr; Janson et al. 2011) of the B2V star Bellatrix (γ Ori) are similar to those of the 32 Ori group. There

are three additional remarkable coincidences among its stellar observables:

(i) Bellatrix's radial velocity (18.2 ± 0.8 km s^{-1}; Barbier-Brossat & Figon 2000) is consistent with the mean group radial velocity of the 32 Ori group (18.6 ± 0.2 km s^{-1}).

(ii) Bellatrix's reddening [$E(B - V) = 0.02$ mag, Friedemann 1992; Zorec et al. 2009; Bhatt & Cami 2015] is a good match for the mean of the 32 Ori group [($E(B - V) = 0.03 \pm 0.01$ mag; see Table 8].[1]

(iii) Bellatrix is the only star in the Northern hemisphere within 100 pc of Earth of spectral type B2 or earlier.

Despite these coincidences, however, we find that Bellatrix's deviant proper motion (see Fig. 1) translates to a 3D velocity of $(U, V, W) = (-14.7 \pm 0.7, -7.1 \pm 0.4, -9.8 \pm 0.3)\,\mathrm{km\,s^{-1}}$ that is inconsistent ($>10\sigma$ in the V component) with the mean velocity of the 32 Ori group shown in Table 2. In light of this kinematic inconsistency, we do not believe there is sufficient evidence at present to include Bellatrix in the group and do not recommend use of the name Bellatrix cluster at this time. Despite this inconsistency, however, we believe further astrometric, spectroscopic and high-contrast imaging of Bellatrix is warranted to see whether it could harbour a dark companion that could be responsible for its deviant velocity.[2]

We hereby present the first large-scale spectroscopic survey for new low-mass members of the 32 Ori group to better understand its stellar population and properties. In Section 2, we discuss our candidate selection process. Section 3 details the medium-resolution optical spectroscopic observations in addition to describing how the spectroscopic properties were determined. In Section 4, we combine various indicators of stellar youth and group membership to identify new bona fide members, and place these in context by comparing them against the findings of previous surveys. Finally, Section 5 synthesizes our stellar census results to discuss the global properties of the 32 Ori group, including its age, circumstellar disc frequency and spatial structure.

2 CANDIDATE SELECTION

Members of a moving group typically cover both a large range of distances and a large area on the sky; unlike compact clusters whose members essentially share the same proper motion, the proper motions and tangential velocities of individual group members can vary systematically and significantly. To identify potential kinematic members of a group, one must therefore project its fixed Galactic *UVW* velocity on to the sky over a range of distances and search for objects sharing a common motion. Furthermore, given the young age of the 32 Ori group, any genuine low-mass members will not only share a common space motion, but will also be overluminous with respect to older MS stars of the same spectral type. In the absence of trigonometric parallaxes (soon to be rectified by

---

[1] Using the revised Johnson Q-method calibration of Pecaut & Mamajek (2013), and the $U - B$ and $B - V$ colours from Mermilliod (2006), we independently estimate the reddening of Bellatrix to be $E(B - V) = 0.017$ mag.
[2] Bellatrix has a mass of $\sim 8.7\,\mathrm{M_\odot}$ (Hohle, Neuhäuser & Schutz 2010), and its projected tangential velocity is peculiar compared to the 32 Ori group velocity by $\Delta\mu_\alpha$, $\Delta\mu_\delta \simeq -16, +20$ mas yr^{-1} (~ 12 km s^{-1} if the star is actually at $d \simeq 93$ pc), with negligible difference in radial velocity. A normal dwarf, white dwarf or neutron star companion cannot reconcile this velocity offset and the consistency of Bellatrix's proper motion over the past decades. The star is too bright for *Gaia* DR1, but the revised *Hipparcos* catalogue (van Leeuwen 2007) reports a seven-parameter solution for Bellatrix with a 2.5σ significance acceleration in μ_α (4.85 ± 1.94 mas yr^{-2}) and negligible acceleration in μ_δ. Bellatrix's velocity and properties can be reconciled with 32 Ori group membership if it is in a face-on orbit perturbed by a distant (a $\sim 10^2$ au, $P \sim$ centuries) black hole companion. We are currently investigating Bellatrix further to test this idea.
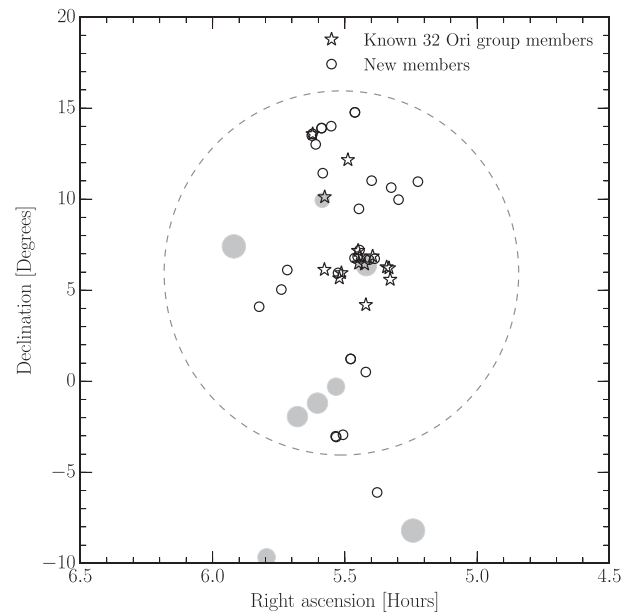

Figure 3. Spatial distribution of the 15 known stellar members of the 32 Ori group listed in Table 1, in addition to the 30 new members we have identified in this study. The dashed circle denotes our $10°$ search radius and the large grey circles represent the bright stars outlining the constellation Orion. The new member outside of our search radius is discussed in Section 4.2 and represents confirmation of a previously identified potential member.

Gaia), the combination of proper motions and photometry provides a robust method with which to identify potential group members, while also efficiently removing a substantial number of field interlopers that are naturally included in large area searches (see Kraus et al. 2014; Murphy & Lawson 2015).

2.1 Input catalogues and search criteria

We adopt UCAC4 as our primary input catalogue, which provides positions, absolute proper motions and instrumental magnitudes (in a single, non-standard bandpass similar to R, hereafter termed R_{UCAC}) complete to $\simeq 16$ mag across the entire sky. In addition to these instrumental magnitudes, the catalogue also includes APASS (Henden et al. 2012) DR6 *BVgri* and 2MASS Point Source Catalog (Cutri et al. 2003) JHK_s photometry. Note that as a consequence of the APASS limiting magnitude ($V \simeq 16$ mag), standard *BVgri* photometry is only available for approximately 50 per cent of the sources in UCAC4.

Given the sky positions of the known group members (see Fig. 3), a $10°$ search radius around 32 Ori itself represents a reasonable compromise between survey area and the telescope time required for spectroscopic follow-up. Within this region, UCAC4 returned a total of $\sim 7.1 \times 10^5$ sources. To identify potential kinematic members from this sample, we follow a formalism similar to that described in Murphy & Lawson (2015). Adopting the mean *UVW* velocity for the 32 Ori group,[3] we project this over a range of distances

---

[3] Our selection of candidate members preceded *Gaia* DR1 and so the actual *UVW* velocity we adopted was slightly different to that stated in Table 2, which we present as the current best estimate for the mean group velocity. The omission of the *Gaia* DR1 astrometry modifies the mean group parallax by $+0.27$ mas and the mean group proper motion by -0.4 and 0.0 mas yr^{-1} in $\mu_\alpha\cos(\delta)$ and μ_δ, respectively, which results in a mean space

($50 \leq d \leq 150$ pc, in 1 pc increments) for each object to calculate the expected proper motion and radial velocity, retaining only those objects whose proper motions and kinematic distances satisfied both of the following criteria:

(i) The lowest total difference between the expected and observed proper motion,

$$\Delta_{\rm PM} = \left[(\mu_\alpha \cos \delta_{\rm obs} - \mu_\alpha \cos \delta_{\rm expt})^2 + (\mu_{\delta\, \rm obs} - \mu_{\delta\, \rm expt})^2 \right]^{1/2}, \quad (1)$$

must be ≤ 10 mas yr^{-1}.

(ii) The 'best' kinematic distance corresponding to this proper motion must be $70 \leq d_{\rm kin} \leq 110$ pc.

These thresholds returned 5349 potential kinematic members of the 32 Ori group, each of which had an associated $\Delta_{\rm PM}$, $d_{\rm kin}$ and expected radial velocity. The $d_{\rm kin}$ and $\Delta_{\rm PM}$ limits are somewhat arbitrary, but are motivated by the bona fide members as found in UCAC4 (14/15 with $\Delta_{\rm PM} < 10$ mas yr^{-1} and 13/15 with $70 < d_{\rm kin} < 110$ pc). During the spectroscopic follow-up, we also observed stars whose distance and $\Delta_{\rm PM}$ values fell outside these limits but otherwise resembled strong candidates.

2.2 Colour–magnitude selection

The kinematic distances determined in Section 2.1 must also be consistent with the colour–magnitude diagram (CMD) positions of young, low-mass stars above the MS. Our primary photometric selection was performed using the UCAC4/APASS DR6 M_V, $V - K_{\rm s}$ CMD. Fig. 4 shows the 3730 (out of 5349) potential kinematic members with APASS V- and 2MASS $K_{\rm s}$-band photometry, in addition to known members of the 32 Ori group that satisfy the same kinematic selection criteria. Also plotted is the empirical fit to the $\sim$130-Myr-old Pleiades single-star sequence by Stauffer et al. (2007), corrected for the effects of both distance and extinction ($d = 136$ pc and $A_V = 0.12$ mag from Melis et al. 2014 and Stauffer et al. 1998, respectively). As expected, the vast majority of sources lie below the Pleiades sequence, indicating that they are field stars with coincidental proper motions and not photometric members of the 32 Ori group. However, there are a significant number of candidates above the sequence whose CMD positions are consistent with known members, i.e. their kinematic distances agree with photometric distances for a putative $\sim$25 Myr population. These stars are potential new 32 Ori group members and we selected $\sim$100 of them for spectroscopic follow-up, with a particular emphasis on late-type stars ($V - K_{\rm s} \geq 3$ mag; spectral type $\gtrsim$K4).

Of the 15 known stellar members listed in Table 1, three do not have counterparts in Fig. 4. While 32 Ori itself satisfies both criteria in Section 2.1, it is saturated in APASS V. In contrast, the best-fitting distances for both V1874 Ori and 2MASS J05194398+0535021 fall outside of the allowed range (131 and 116 pc, respectively). The latter member also has $\Delta_{\rm PM} = 12.5$ mas yr^{-1}, but with large (>10 mas yr^{-1}) errors on its UCAC4 proper motion.[4]

Given the incompleteness of APASS $BVgri$ photometry in UCAC4, we also searched for additional low-mass members in

---

motion of $(U, V, W) = (11.9 \pm 0.3, -18.6 \pm 0.4, -9.0 \pm 0.3)$ km s^{-1}. We note, however, that this subtle difference in the adopted UVW velocity does not have a significant impact on the calculated $\Delta_{\rm PM}$ and kinematic distances, on average affecting these at the <1 mas yr^{-1} and <2 pc level, respectively.
[4] If we instead adopt proper motions from URAT1 for V1874 Ori and PPMXL for 2MASS J05194398+0535021 (as found in Table 1 and which has a smaller uncertainty than UCAC4), we calculate distances of 88 and 110 pc, respectively. Both stars would then satisfy the selection criteria.
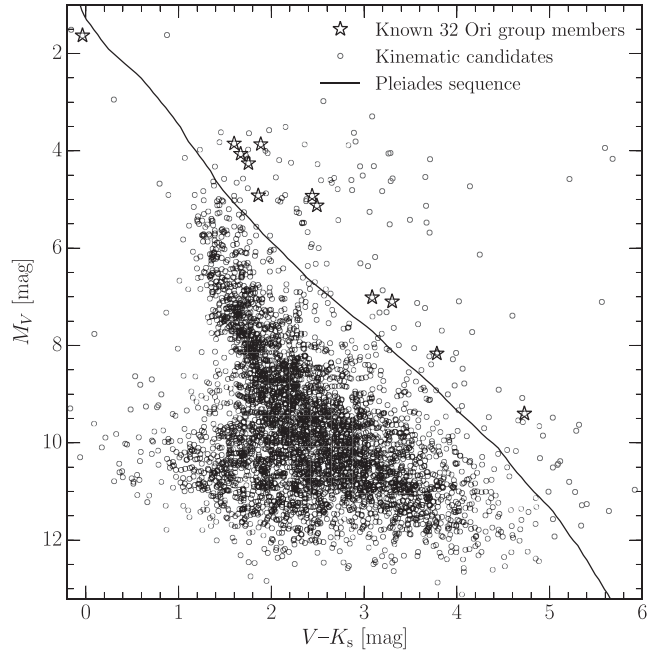

Figure 4. UCAC4/APASS DR6 M_V, $V - K_{\rm s}$ CMD. The circles denote potential kinematic members and the stars are known 32 Ori group members in UCAC4 that satisfy the same kinematic selection criteria (see Section 2.1). The solid line is the empirical fit to the Pleiades single-star sequence by Stauffer et al. (2007) that has been corrected for the effects of both distance and interstellar extinction.

the $M_{R_{\rm UCAC}}$, $R_{\rm UCAC} - K_{\rm s}$ CMD using the stars selected in Fig. 4 as a reference, and identified $\sim$30 additional candidates with consistent CMD positions not present in the M_V, $V - K_{\rm s}$ diagram. Furthermore, we also looked for potential members in the First U.S. Naval Observatory Robotic Astrometric Telescope Catalog (URAT1; Zacharias et al. 2015), which extends approximately 2 mag fainter than UCAC4 in an almost identical non-standard pseudo-R bandpass. We used the same method as above, but allowed a $\Delta_{\rm PM} < 15$ mas yr^{-1} limit due to the two-epoch astrometry having larger proper motion uncertainties. From a similar kinematic and CMD analysis, we identified another $\sim$20 candidates only present in URAT1 down to $R \approx 16$ mag, giving a total of $\sim$150 potential members from the combined searches.

The fainter $R_{\rm UCAC}$ and URAT1 samples are crucial for better estimating the age of the group. The limiting magnitude of APASS is $V \simeq 16$ mag, which at a distance of 90 pc, corresponds to the expected location of the lithium depletion boundary (LDB) in a $\sim$25 Myr population. Only by confirming fainter Li-rich members can we can identify the precise position of the 32 Ori group LDB and calculate a semifundamental (Soderblom et al. 2014) age for the group (see Section 5.3).

3 SPECTROSCOPIC OBSERVATIONS AND DATA ANALYSIS

To unambiguously differentiate between genuine 32 Ori group members and field interlopers or other contaminants, additional spectroscopic diagnostics are required. These typically include measuring radial velocities to ascertain whether candidates share similar three-dimensional space motions, as well as identifying spectroscopic features associated with stellar youth (e.g. Li I 6708 Å absorption and Hα emission).

We observed 124 candidate members (plus 11 of the known members listed in Bell et al. 2015) in four runs between 2015 September and 2016 February using the Wide Field Spectrograph (WiFeS; Dopita et al. 2007) on the ANU 2.3-m telescope at Siding Spring Observatory (SSO). Poorer than expected conditions meant we were unable to observe all of the faintest ($V > 15$ mag) candidates and so we prioritized objects with small Δ_{PM} values, CMD or sky positions similar to known members and candidates coincident with the *ROSAT* X-ray sources (Voges et al. 1999). We later took observations in 2016 October and 2017 January to revisit several possible spectroscopic binaries identified in earlier runs.

WiFeS is an image-slicing integral field spectrograph with a nominal 25×38 arcsec field of view and 0.5 arcsec sampling along $25\ 38 \times 1$ arcsec slitlets. Observations were made in half-field (12×38 arcsec) 'stellar' mode with $2 \times$ spatial binning (1 arcsec spaxels; well matched to typical 1.5–2.5 arcsec SSO seeing). The $R7000$ grating and $RT480$ dichroic gave a resolution of $\lambda / \Delta\lambda \approx 7000$ and wavelength coverage from 5300 to 7000 Å. The field of view was aligned to the parallactic angle prior to each exposure, with exposure times up to 3×1200 s. In addition to science targets, we also obtained spectra for 4–10 FGKM radial velocity standards each night from the list of Nidever et al. (2002) and white dwarf flux calibrators following Bessell (1999).

After basic image processing, we used IRAF, FIGARO and PYTHON routines to rectify, extract, wavelength-calibrate and combine the three to six image slices (depending on seeing) that contained the majority of the stellar flux. The slices were treated like long-slit spectra and individually extracted and wavelength calibrated against NeAr arc frames taken following each exposure. The rms of the final wavelength solution in all cases was better than 0.02 Å. Typical signal-to-noise ratios were 50–100 around Hα and Li I, decreasing to ~20 for the faintest candidates. Table 3 (the full version of which is available as Supporting Information with the online version of the paper) details our spectroscopic measurements for the observed candidates and known members listed in Bell et al. (2015). Typical WiFeS/$R7000$ spectra of several new M dwarf 32 Ori group members confirmed in this work are shown in Fig. 5.

3.1 Spectral types

Spectral types for each candidate were first estimated by visual comparison against the Pickles (1998) stellar spectral flux library and the Sloan Digital Sky Survey (SDSS) average M dwarf templates of Bochanski et al. (2007), with the WiFeS spectra Gaussian-smoothed to the approximate resolution of the templates prior to comparison. This analysis showed a substantial fraction of the candidates were clearly reddened, motivating us to fit their spectra to the templates with interstellar reddening as a free parameter. For this, we adopted the Cardelli, Clayton & Mathis (1989) reddening law and a total-to-selective extinction ratio of $R_V = 3.1$ and calculated the best-fitting reddening [in the range $0 < E(B - V) < 3$ mag, in 0.05 mag increments], after resampling the template on to the same wavelength array as the star. The unreduced χ^2 statistic was used as the goodness of fit.

The resulting spectral types for all candidates are listed in Table 3, with the estimated reddenings provided in the electronic version of the table (see also Table 8 for the early-type members). Given the modest wavelength range of the WiFeS data, spectral type coverage of the Pickles library and degeneracies with reddening, we estimate these types are accurate to ± 1–2 subtypes for A-, F-, G- and K-type candidates. The homogeneity and high quality of the SDSS

M dwarf templates permit spectral types for these candidates to approximately half a subtype.

3.2 Radial velocities

Radial velocities for each candidate were measured by cross-correlation over 5500–6500 Å against standards of similar spectral type observed that run using a PYTHON implementation of the FXCOR algorithm (Tonry & Davis 1979). Following the procedure described in Murphy & Lawson (2015), each spectrum was first resampled on to a log-linear wavelength scale and normalized by subtracting a boxcar-smoothed copy and dividing by the standard deviation. The waveforms were then cross-correlated and a Gaussian fitted to the cross-correlation function (CCF) peak, before transforming to a heliocentric frame. The velocities reported in Table 3 are the mean and standard deviation against standards observed that run. Repeat and standard star observations demonstrate that the instrument and this technique provide an external velocity precision of $\lesssim 1$ km s^{-1} for bright stars. For the faintest candidates in Table 3, this falls to 2–3 km s^{-1} per exposure.

3.2.1 Spectroscopic binaries and fast rotators

Six candidates (HD 37825, BD+08 900B, 2MASS J05442447+0502114, 2MASS J05363692+1300369, 2MASS J05320596−0301159, 2MASS J05561307+0803034) and the previously known 32 Ori group members HD 35499 and HD 35695 showed average CCF widths significantly larger than other stars (FWHM $\gtrsim 2.5$ px; see Murphy & Lawson 2015), with BD+08 900A and the known member 2MASS J05234246+0651581 borderline cases. This broadening can be attributed to either fast rotation or unresolved spectroscopic binarity at the modest ($c\Delta\lambda/\lambda \approx 45$ km s^{-1}) velocity resolution of WiFeS (see discussion in Murphy & Lawson 2015). Three of these stars – HD 37825, 2M0536+1300 and 2M0556+0803 – showed double line cores and broad, asymmetric (though unresolved) CCFs indicative of double-lined spectroscopic binary systems (SB2). Notably, the 2016 October and 2017 January CCFs of HD 37825 were clearly resolved into two near-equal amplitude peaks (the latter spectrum showing the system to be an SB3 with a weak tertiary component; see Fig. 6), while the 2016 February 21 spectrum had much narrower, single profiles, ostensibly close to the systemic velocity (RV ≈ 28 km s^{-1}).

In the absence of resolved double lines, the origin of the broadening seen in the other stars is less clear. Given their smoother spectral features and symmetric CCFs, it is likely HD 35499, HD 35695, 2M0532−0301 and 2M0544+0502 are fast rotators ($v \sin i \gtrsim 45$ km s^{-1}), while BD+08 900B may be a binary (with BD+08 900A more likely a fast rotator). Higher resolution observations are necessary to confirm these predictions.

Of the 21 candidates or previously known members observed more than once with WiFeS (see Tables 4 and 5), eight non-SB2s have maximum radial velocity differences larger than 5 km s^{-1} and therefore may be single-lined (SB1) spectroscopic binaries. One of these stars (2MASS J05525572−0044266) is a known ~0.86 d period eclipsing binary (Drake et al. 2014, see Section 4.4.1), while three more have broad CCFs (and thus less precise velocities), yielding differences marginally greater than 5 km s^{-1} (HD 35499, 2M0532−0301 and 2M0544+0502). The Li-rich candidate 2MASS J05350092+1125423 (RV$_{expt}$ = 17.4 km s^{-1}) was observed twice in 2016 February (19.6 and 10.9 km s^{-1}, $\Delta t = 3$ d),

Table 3. Spectroscopic parameters and membership assignments for the candidate members and 11 known members of the 32 Ori group observed with WiFeS. Four additional early-type stars and a brown dwarf confirmed as members but not observed in this work are also included. HD 36002 and SCR 0522−0606 were not in the original candidate list but were added and confirmed during observations. The full table, which also includes possible and non-members as well as derived $E(B - V)$ values and object-specific comments (omitted in the print version due to space restrictions), is available as Supporting Information with the online version of the paper.

THOR no.	2MASS J designation	Other name	V (mag)	Ref.	K_s (mag)	$\mu_\alpha \cos(\delta)$ (mas yr^{-1})	μ_δ (mas yr^{-1})	Ref.	d_{kin} (pc)	d_{trig} (pc)	Ref.	RV (km s^{-1})	Δ_{RV} (km s^{-1})	SpT	EW[Hα] (Å)	EW[Li] (mÅ)	Membership RV,Hα,Li	Final
1	05304706+0556536	32 Ori	4.20	1	4.61	12.9 ± 1.0	−28.1 ± 1.0	2	102	93^{+6}_{-5}	3	–	–	B5+B7	–	–	–,–,–	Y
2	05263883+0652071	HR 1807	6.41	4	6.41	9.2 ± 1.0	−33.2 ± 1.0	2	92	92 ± 4	3	–	–	B9.5	–	–	–,–,–	Y
3A	05265999+0710131	HD 35714	7.03	5	6.75	8.4 ± 1.0	−34.2 ± 1.0	2	91	94^{+3}_{-4}	6	–	–	A3	–	–	–,–,–	Y
3B	05343842+0607367	HD 36823	7.73	5	7.14	9.0 ± 0.6	−31.1 ± 0.5	2	95	102 ± 5	6	–	–	A7.5	–	–	–,–,–	Y
4A	05284209+0113369	HD 36002	7.46	5	6.71	6.9 ± 1.0	−25.6 ± 1.0	2	105	109^{+6}_{-5}	6	SB2	–	A7	14	~70	?,?,?	Y
4B	05284050+0113333		14.74	7	10.19	8.8 ± 5.8	−26.6 ± 5.8	8	99	–	8	18.4 ± 1.0	−1.5	M3.5	−4.8	<50	Y,?,Y	Y
5	05251457+0411482	HD 35499	8.66	5	7.50	6.1 ± 0.6	−27.5 ± 0.8	5	106	105^{+8}_{-6}	9	20.6 ± 2.6^a	+1.4	F4	8.0	160	Y,?,Y	Y
6	05311570+0539461	HD 36338	8.52	5	7.40	9.3 ± 0.6	−31.1 ± 0.9	5	95	96 ± 5	9	21.3 ± 0.2	+2.4	F4.5	7.0	110	Y,?,Y	Y
7	05265202+0628227	HD 35695	9.27	5	7.71	9.2 ± 0.8	−36.1 ± 1.2	5	84	–	–	20.0 ± 0.3^a	+1.4	F9	5.0	280	Y,?,Y	Y
8A	05371844+1334525	HD 245567	9.54	5	7.59	7.2 ± 0.9	−33.5 ± 0.8	5	104	–	–	16.0 ± 1.3	−0.8	G5	−0.2^b	265	Y,?,Y	Y
8B	05372061+1335310		14.96	7	10.07	6.9 ± 6.2	−30.8 ± 5.7	2	113	–	–	15.7 ± 0.8	−1.1	M3	−4.8	<30	Y,?,Y	Y
9	05343491+1007062	HD 245059	9.96	5	7.41	10.1 ± 1.3	−35.0 ± 1.2	2	92	–	–	19.4 ± 1.1	+1.6	G7	−0.2	285	Y,?,Y	Y
10	05203182+0616115	TYC 112-1486-1	11.87	7	8.57	9.5 ± 1.8	−32.8 ± 2.1	2	92	99^{+14}_{-11}	9	21.1 ± 0.3	+2.5	K3	−1.2	500	Y,?,Y	Y
11	05200029+0613036	TYC 112-917-1	11.66	7	8.57	9.4 ± 1.9	−34.7 ± 2.1	2	86	–	–	21.0 ± 0.3	+2.4	K4	−0.3	470	Y,?,Y	Y
12	05234246+0651581	1RXS J052342.7+065156	12.81	7	9.03	7.8 ± 2.3	−36.6 ± 2.8	2	85	–	–	18.3 ± 4.2^a	−0.2	K6.5	−5.0	580	Y,?,Y	Y
13	05291899+1209295	V1874 Ori	13.22	7	9.19	2.9 ± 2.1	−26.7 ± 3.0	2	131	–	–	22.4 ± 0.3	+5.3	K6.5	−1.7	380	Y,?,Y	Y
14A	05351761+1354180		13.53	7	9.15	7.0 ± 4.4	−30.2 ± 9.4	2	116	–	–	18.1 ± 2.8^a	+1.4	M1.5	−1.7	180	Y,?,Y	Y
14B	05351625+1353594	1RXS J053516.6+135404	14.95	10	10.39	7.6 ± 4.3	−31.8 ± 4.6	10	110	–	–	19.2 ± 1.0	+2.5	M3.5	−6.1	<40	Y,?,Y	Y
15	05330574+1400365	1RXS J053306.7+140011	13.80	7	9.35	9.4 ± 2.4	−37.4 ± 2.2	7	94	–	–	19.2 ± 2.9^a	+2.5	M2	−2.0	160	Y,?,Y	Y
16	05430354+0606340	1RXS J054304.3+060646	14.98	7	10.29	11.5 ± 5.4	−25.2 ± 5.9	7	114	–	–	21.0 ± 0.9	+2.1	M2.5	−2.9	<50	Y,?,Y	Y
17A	05274313+1446121	1RXS J052743.4+144609	14.13	7	9.10	8.6 ± 3.8	−41.1 ± 3.8	2	87	–	–	15.8 ± 1.1^a	−0.6	M3	−10.3^b	<100	Y,?,Y	Y
17B	05274404+1445584		16.26	10	10.97	6.5 ± 6.0	−44.4 ± 6.7	10	82	–	–	15.4 ± 0.8	−1.0	M5	−5.9	580	Y,?,Y	Y
18	05224069−0606238	SCR 0522−0606	14.27	7	9.13	17.0 ± 3.2	−21.1 ± 3.3	2	88	–	–	25.6 ± 1.9^a	+4.3	M3	−7.0	<20	Y,?,Y	Y
19	05253253+0625336	1RXS J052532.3+062534	14.51	7	9.78	8.0 ± 5.8	−28.2 ± 6.1	7	107	–	–	19.6 ± 0.4^a	+1.0	M3	−6.6	<20	Y,?,Y	Y
20	05192941+1038081	1RXS J051930.4+103812	14.66	7	9.77	8.5 ± 7.1	−32.9 ± 5.1	2	101	–	–	17.7 ± 0.8^a	+0.3	M3	−7.1	<80	Y,?,Y	Y
21	05251517+0030232	1RXS J052515.0+003027	14.85	7	9.93	10.3 ± 5.8	−24.7 ± 6.0	2	103	–	–	19.9 ± 0.7	−0.1	M3	−9.7^b	<20	Y,?,Y	Y
22	05492632+0405379	1RXS J054926.3+040541	14.96	7	10.07	11.2 ± 5.5	−33.3 ± 5.9	7	84	–	–	20.9 ± 1.0	+1.4	M3	−2.5	<50	Y,?,Y	Y
23	05442447+0502114	1RXS J054424.7+050153	15.08	7	10.24	15.8 ± 5.4	−28.4 ± 5.8	2	98	–	–	24.4 ± 2.6^a	+5.2	M3	−4.4	<30	Y,?,Y	Y
24	05194398+0535021		15.13	7	10.00	−4.2 ± 16.4	−29.3 ± 13.3	7	116	–	–	15.1 ± 0.8	−3.6	M3	−15.0	<20	Y,?,Y	Y
25	05132631+1057439		15.25	7	10.22	7.3 ± 5.9	−30.2 ± 5.9	2	113	–	–	17.0 ± 0.7	−0.2	M3	−5.2	<50	Y,?,Y	Y
26	05302546−0256255		15.65	7	10.66	12.1 ± 2.7	−25.7 ± 3.2	2	88	–	–	25.1 ± 1.2	+4.3	M3	−10.0^b	<90	Y,?,Y	Y
27	05274855+0645459	1RXS J052748.7+064544	14.75	7	9.47	10.9 ± 5.9	−29.1 ± 6.3	2	102	–	–	18.8 ± 0.8	+0.2	M4	−6.6	<50	Y,?,Y	Y
28	05264886+0928055		15.64	11	10.47	6.7 ± 5.3	−32.7 ± 6.1	11	100	–	–	22.4 ± 0.8	+4.6	M4	−3.9	<70	Y,?,Y	Y
29	05231438+0643531	1RXS J052315.0+064412	15.86	10	10.76	3.2 ± 5.9	−28.4 ± 5.9	8	113	–	–	21.0 ± 0.6^a	+2.4	M4	−3.3	<50	Y,?,Y	Y
30	05313290+0556597	1RXS J053132.6+055639	15.90	7	10.53	−0.8 ± 5.7	−37.4 ± 5.7	8	85	–	–	24.7 ± 1.1	+5.9	M4.5	−6.4	<80	Y,?,Y	Y
31	05363692+1300369		16.10	11	10.39	4.6 ± 4.4	−36.3 ± 4.6	11	96	–	–	18.0 ± 6.6^a	+1.0	M4.5	−17	350–500	Y,?,Y	Y
32	05264073+0712255		16.32	7	10.76	1.9 ± 4.1	−32.8 ± 4.4	7	99	–	–	18.8 ± 0.5	+0.4	M4.5	−4.6	600	Y,?,Y	Y
33	05315786−0303367		13.85	7	8.54	4.2 ± 6.6	−34.8 ± 4.9	2	71	–	–	23.1 ± 1.0	+2.3	M5^c	−9.0	<150	Y,?,Y	Y
34	05320596−0301159		15.61	7	9.70	9.2 ± 4.9	−27.4 ± 4.9	2	85	–	–	23.6 ± 2.7^a	+2.8	M5	−11.0	650	Y,?,Y	Y
35	05174962+0958221		16.63	7	10.84	22.3 ± 5.9	−33.3 ± 5.9	8	89	–	–	18.1 ± 1.6	+0.6	M5	−6.9	530	Y,?,Y	Y
36	05235565+1101027	1RXS J052355.2+110110	16.65	11	10.78	7.4 ± 6.3	−30.3 ± 6.3	11	110	–	–	18.1 ± 1.2	+0.7	M5	−5.8	680	Y,?,Y	Y
37	05350092+1125423		16.84	11	11.02	7.1 ± 6.6	−43.0 ± 6.7	2	79	–	–	17.8 ± 4.0^a	+0.4	M5	−6.7^b	700	Y,?,Y	Y

Table 3 – *Continued*

THOR no.	2MASS J designation	Other name	V (mag)	Ref.	K_s (mag)	$\mu_\alpha\cos(\delta)$ (mas yr^{-1})	μ_δ (mas yr^{-1})	Ref.	d_{kin} (pc)	d_{trig} (pc)	Ref.	RV (km s^{-1})	Δ_{RV} (km s^{-1})	SpT	EW[Hα] (Å)	EW[Li] (mÅ)	Membership RV,Hα,Li	Final
38	05243009+0640349		16.97	10	11.13	8.8±6.0	−36.8±6.0	8	84	–	–	16.1±1.0	−2.4	M5	−14.0	750	Y,?,Y	Y
39	05270634+0650377		17.60	11	11.64	10.1±5.9	−35.8±5.9	8	85	–	–	20.8±1.0	+2.3	M5	−8.5	650	Y,?,Y	Y
40	05373000+1329344		16.51	10	10.78	3.2±6.4	−32.1±6.4	8	110	–	–	18.5±1.2	+1.6	M5.5	−13.2	630	Y,?,Y	Y
41	–	*WISE* J052857.68+090104.4	–	–	14.97^d	−11.0±10.0	−39.0±12.0	12	93	–	–	–	–	L1	–	–		Y

Column descriptions for the online version of the Table: column 1 gives the 32 Ori (THOR) member number assigned in this study. Columns 2 and 3 list the 2MASS object identifier and the other commonly adopted name. Columns 4 and 5 provide the *V*-band magnitude and the source reference. Column 6 gives the 2MASS Point Source Catalog (PSC; Cutri et al. 2003) K_s-band magnitude, unless otherwise stated. Columns 7–9 list the proper motion in the right ascension, declination used in the selection of candidate members and the source reference. Columns 10–12 provide the best-fitting kinematic distance as calculated in Section 2.1, available literature trigonometric parallax distances and the source reference. Columns 13 and 14 give the measured radial velocity and radial velocity residual. Columns 15 and 16 list the spectroscopic spectral type and best-fitting $E(B - V)$ reddening. Columns 17 and 18 provide the measured Hα and Li EWs. Columns 19 and 20 give the combined radial velocity, Hα emission, Li absorption membership diagnostics and the final membership assignment. Column 21 lists additional object-specific comments.
References for the *V*-band photometry, proper motions and trigonometric parallax distances: (1) Mermilliod (2006); (2) Zacharias et al. (2013); (3) van Leeuwen (2007); (4) Hauck & Mermilliod (1998); (5) *Tycho-2*
V_T photometry converted to Johnson *V* following Mamajek, Meyer & Liebert (2006); (6) Weighted mean of revised *Hipparcos* reduction (van Leeuwen 2007) and *Gaia* DR1 (Gaia Collaboration et al. 2016)
parallaxes; (7) Henden et al. (2016); (8) Zacharias et al. (2015); (9) *Gaia* DR1; (10) Zacharias et al. (2005); (11) Dolan & Mathieu (2002); (12) Burgasser et al. (2016). Note that all parallax measurements from
Gaia DR1 include the additional ±0.3 mas systematic uncertainty as discussed in Gaia Collaboration et al. (2016).
^{a}Mean velocity and standard deviation from multiple epochs (see Table 4 for individual measurements).
^{b}Spectrum also showed strong He I 5876 and/or 6678 Å emission.
^{c}5 arcsec visual binary; WiFeS spectrum is unresolved.
^{d}The K_s-band magnitude from the 2MASS Point Source Reject Table (Cutri et al. 2003, see also Burgasser et al. 2016).

with further observations in 2016 October (21.0 km s^{-1}) and 2017 January (19.5 km s^{-1}). Given the agreement of the three other epochs, with no other indications of binarity, it is likely that the second February velocity was erroneous. The known K6.5 member 2M0523+0651 (RV$_{expt}$ = 18.5 km s^{-1}) has two WiFeS velocities separated by 442 d that agree and a third that is discrepant by ∼9 km s^{-1}, well outside the expected errors. Alcalá et al. (2000) reported a 18.4 ± 1.0 km s^{-1} velocity from a high-resolution ($R \approx 30\,000$) spectrum that agrees with the expected velocity. Interestingly, that study noted 2M0523+0651 may be a spectroscopic binary based on an asymmetric CCF and we too find a somewhat broadened CCF in our observations. Finally, the Li-rich, early M-type candidates 2MASS J05351761+1354180 and 2MASS J05330574+1400365 both have velocity differences of ∼7 km s^{-1} over three epochs. They do not show broadened CCFs and their mean velocities are close to those expected of bona fide members.

3.3 Hα and Li equivalent widths

Young stars are predominantly active and one of the most common diagnostics of activity is the Balmer Hα line at 6563 Å. For late-type stars (spectral type $\gtrsim$ M0) Hα is typically seen in emission to ages of several Gyr (e.g. Gizis, Reid & Hawley 2002), whereas in early and solar-type stars, it can be seen in various levels of emission or absorption depending on activity. We measured the Hα equivalent width (EW) of our candidates by fitting a single Gaussian or Voigt profile with linear continuum to the emission/absorption feature. For stars where the line could not be well fitted analytically, EW[Hα] was calculated by direct integration of the line profile. Due to uncertainties in the placement of the continuum and integration limits, we estimate uncertainties of up to 1 Å in the measured EW[Hα] values. Several of the M-type stars in our sample also showed strong He I emission at 5876 and 6678 Å. This is chromospheric in nature and is observed in active M-dwarfs with ages of up to several Gyr (Gizis et al. 2002).

Another key indicator of stellar youth is the resonant Li I 6708 Å absorption feature. As a coeval group of young stars contracts towards the zero-age MS their core temperatures increase until at ∼3 × 10^6 K Li fuses. Such temperatures can be reached in either fully convective mid- to late-M dwarfs or at the base of the convective zone in late-K/early-M dwarfs. For stars between these luminosities, rapid Li depletion ensues and the Li I feature is no longer visible. At an age of ∼25 Myr, we expect Li to be fully depleted in stars with spectral types between ∼M1.5 and M4.5; however, it should still be present in both earlier and later spectral types (see e.g. Mentuch et al. 2008; Jeffries et al. 2013). As in the case of Hα, we determined EW[Li] by Gaussian profile fitting if the line was present and estimated an upper limit from the local pseudo-continuum if it was not. No attempt was made to deblend Li I from the nearby Fe I feature at 6707.4 Å, which is unresolved at our resolution and is typically much weaker (EW[Fe] $\lesssim$ 30 mÅ; Soderblom et al. 1993) compared to the expected EW[Li] of 32 Ori group members. WiFeS EW[Hα] and EW[Li] values for all observed candidate and known members of the 32 Ori group are listed in Table 3.

4 THE LOW-MASS POPULATION OF THE 32 ORI GROUP

4.1 Newly identified members

While any one of the diagnostics discussed in Section 3 could be used to assign membership of a candidate to the 32 Ori group, this
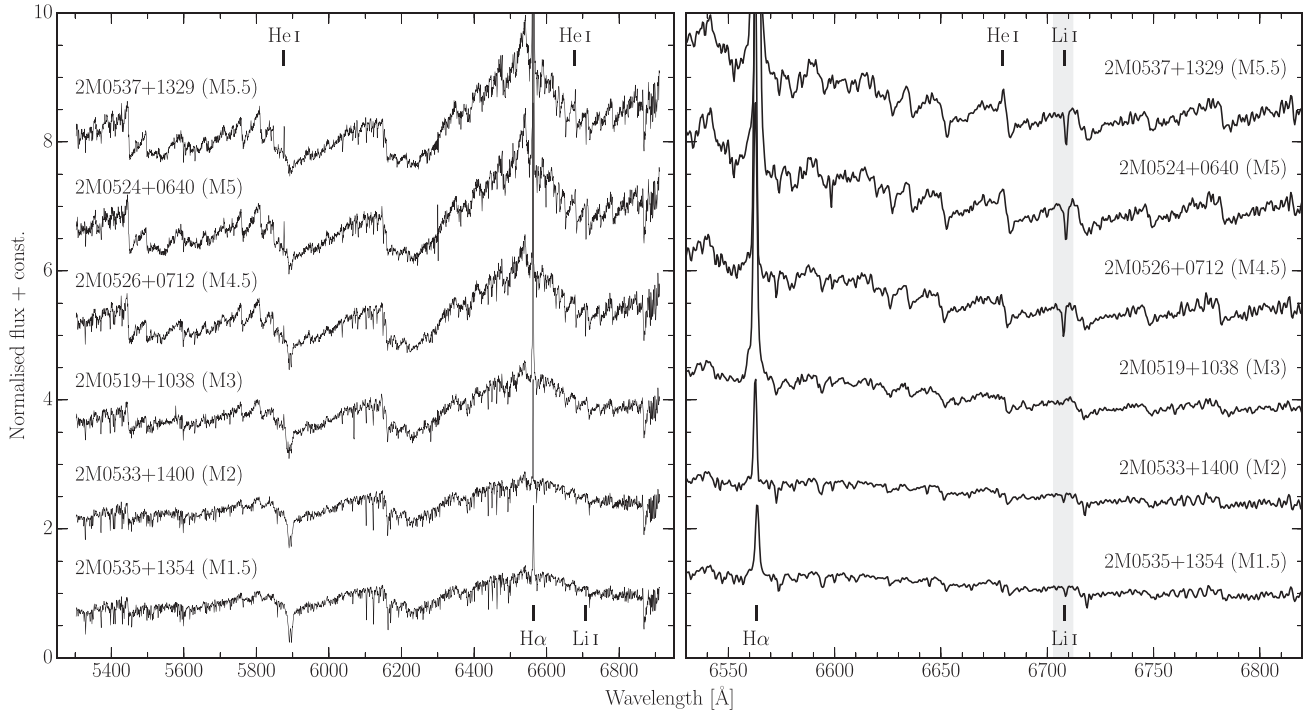
Figure 5. WiFeS/*R*7000 spectra for a selection of new M dwarf 32 Ori group members identified in this study. Fluxes are normalized around 6100 Å and key youth indicators are labelled. Li ɪ 6708 Å absorption decreases in strength with decreasing effective temperature through the early-M spectral types, before sharply returning to undepleted levels below the ∼25 Myr LDB at around M4.5 (see also Fig. 7).
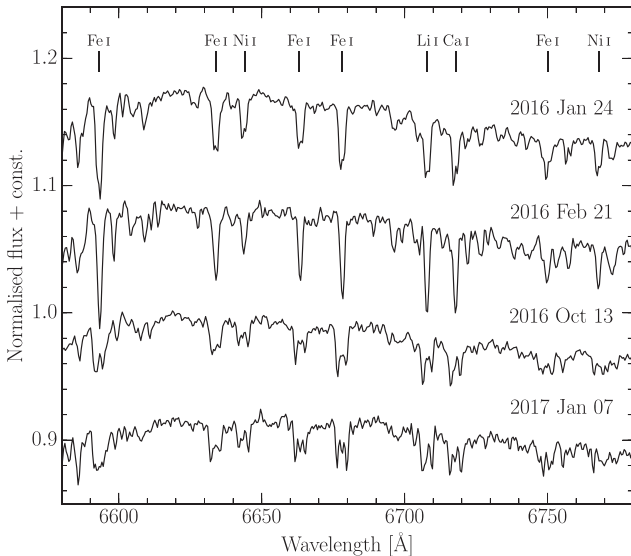

Figure 6. Li ɪ-region spectra of the new SB3 system and possible member HD 37825 (spectral type F5), showing clear evolution of its neutral metal lines with time. The 2016 February spectrum is single-lined (RV ≈ 28 km s^{-1}), while in 2016 October and 2017 January, it is resolved into three components (only two of which are visible in the CCF). The two main components are marginally resolved in 2016 January.

increases the risk of erroneously including a member, which when assessed using an alternative diagnostic, is an obvious non-member. The most discriminating diagnostic to differentiate between young and older stars is the presence of Li; however, this is only valid over a small range of spectral types (see e.g. Jeffries 2006). In addition,

stellar activity as traced by Hα emission is not solely restricted to the youngest stars, with older K- and M-type field stars also exhibiting elevated levels of activity (see e.g. West et al. 2011) and so while the presence of Hα is necessary, it alone does not provide a reliable membership diagnostic. Finally, although one would expect stars with the same space motion as the 32 Ori group to be likely members, within a given sample there will always be a small fraction of older field stars that are comoving purely by coincidence. In contrast, radial velocities of genuine short-period binary members based on single-epoch spectra will, in the majority of cases, suggest that these are not comoving.

To minimize the number of potential interlopers in our final membership, we combine all three spectroscopic diagnostics (Li, Hα, RV) in conjunction with the proper motion match (Δ_{PM}) and kinematic distance determined in Section 2.1. We adopt a threshold of EW[Li] ≥ 100 mÅ across the entire spectral type range of our sample as an indicator of youth, whereas those stars with measured EW[Li] < 100 mÅ for spectral types ≤ K5 and ≥ M5 are deemed to be older field interlopers. Although there is a range of observed Hα emission levels in both young coeval populations and older field stars, young stars do exhibit a lower envelope of Hα emission (see e.g. Kraus et al. 2014 in the slightly older Tucana–Horologium association; hereafter Tuc–Hor) and so we classify any star with emission below this envelope as an older field star. To illustrate these criteria, the EW[Li] and EW[Hα] values of observed candidates and members of the 32 Ori group are plotted as a function of $V - K_s$ colour in Figs 7 and 8.

Fig. 7 shows the Li depletion pattern of the 32 Ori group compared to other nearby young moving groups. While the overall trend for all such groups is very similar for G-type stars and earlier, as one moves into the K- and M-type regime the older groups clearly show evidence of significant Li depletion at earlier spectral types

Table 4. Individual WiFeS radial velocities of candidates observed at more than one epoch. Stars with a THOR number (Column 1) are confirmed members of the 32 Ori group. The final column denotes whether the star is a confirmed or suspected spectroscopic binary. Three additional resolved SB systems are listed with their component velocities in Table 5.

THOR no.	Name	Epoch (UT)	RV (km s^{-1})	SB?
5	HD 35499	2015 Oct 25	23.2 ± 0.8	N
		2016 Oct 13	18.0 ± 0.6	
7	HD 35695	2015 Oct 25	20.3 ± 0.5	N
		2016 Oct 13	19.7 ± 1.3	
12	2M0523+0651	2015 Oct 23	15.0 ± 2.2	SB2?
		2016 Oct 13	24.2 ± 1.4	
		2017 Jan 07	15.6 ± 1.9	
14A	2M0535+1354	2016 Jan 23	21.5 ± 0.7	SB1?
		2017 Jan 07	18.1 ± 0.9	
		2017 Jan 07	14.7 ± 1.2	
15	2M0533+1400	2015 Oct 19	23.1 ± 0.6	SB1?
		2015 Oct 20	18.5 ± 0.7	
		2017 Jan 07	16.1 ± 1.2	
17A	2M0527+1446	2015 Oct 20	14.4 ± 0.8	N
		2016 Jan 26	17.0 ± 1.0	
		2016 Jan 30	16.0 ± 1.0	
18	SCR 0522−0606	2016 Oct 14	23.7 ± 1.7	SB2
		2017 Jan 07	27.4 ± 1.7	
19	2M0525+0625	2015 Oct 23	19.2 ± 0.7	N
		2015 Oct 25	20.0 ± 0.6	
20	2M0519+1038	2015 Oct 19	18.4 ± 1.1	N
		2015 Oct 19	16.9 ± 0.9	
23	2M0544+0502	2016 Jan 23	21.8 ± 1.8	N
		2016 Oct 14	26.9 ± 1.6	
29	2M0523+0643	2016 Jan 25	20.4 ± 1.0	N
		2016 Jan 29	21.5 ± 0.9	
31	2M0536+1300	2016 Jan 25	16.3 ± 1.5	SB2
		2016 Oct 13	28.4 ± 2.1	
		2016 Oct 14	17.4 ± 2.4	
		2017 Jan 07	10.0 ± 3.0	
34	2M0532−0301	2016 Jan 29	26.2 ± 1.3	N
		2017 Jan 08	20.9 ± 2.6	
37	2M0535+1125	2016 Feb 18	19.6 ± 1.9	N?
		2016 Feb 21	10.9 ± 1.4	
		2016 Oct 14	21.0 ± 1.7	
		2017 Jan 08	19.5 ± 0.9	
–	BD+08 900A	2015 Sep 28	19.3 ± 1.1	N
		2015 Sep 28	20.6 ± 1.0	
		2016 Oct 13	18.9 ± 0.7	
		2017 Jan 07	22.3 ± 4.2^a	
		2017 Jan 07	19.3 ± 4.5^a	
–	BD+08 900B	2015 Sep 28	20.8 ± 1.3	SB2?
		2015 Sep 28	17.9 ± 0.9	
		2016 Oct 13	20.7 ± 0.7	
		2017 Jan 07	21.3 ± 5.9^a	
		2017 Jan 07	20.9 ± 6.9^a	
–	HD 243086	2016 Jan 24	23.7 ± 1.7	N
		2016 Feb 21	21.9 ± 1.0	
–	2M0556+0803	2016 Feb 21	28.3 ± 1.3	SB2
		2017 Jan 09	23.9 ± 2.7	

^{a}Cross-correlated against M-dwarf standards as no F-type standards were observed during run.

Table 5. Individual radial velocities for the three systems that could be resolved into two components. HD 37825 is a clear SB3 system (see Fig. 6) with a weaker third component not resolved in the 2017 Jan CCF. 2M0552−0044 shows a single-peaked CCF but has a variable, double-peaked Hα emission line from which a velocity offset was estimated and added to the primary velocity.

Name	Epoch (UT)	RV$_1$ (km s^{-1})	RV$_2$ (km s^{-1})
HD 36002 (SB2)	2017 Jan 11	+69.8 ± 3.3^a	−32.8 ± 3.0^a
	2017 Jan 11	+58.2 ± 2.0^a	−27.0 ± 3.0^a
HD 37825 (SB3)	2016 Jan 24	25.3^b	–
	2016 Feb 21	+28.1 ± 0.8	–
	2016 Oct 13	−42.5 ± 2.5	+95.3 ± 1.9
	2017 Jan 07	−42.1 ± 3.0^a	+101.9 ± 1.8^a
2M0552−0044 (SB1+Hα)	2015 Oct 23	+65.5 ± 0.7	−99.5 ± 5.4
	2016 Oct 14	−39.3 ± 1.5	+160.7 ± 5.6
	2017 Jan 07	+18.4 ± 1.6	–
	2017 Jan 07	−34.0 ± 1.0	+136.0 ± 5.5
	2017 Jan 08	−26.4 ± 0.8	+163.6 ± 5.4
	2017 Jan 08	−16.6 ± 1.0	+133.4 ± 5.5
	2017 Jan 09	−22.9 ± 0.7	+157.1 ± 5.4

^{a}Cross-correlated against M-dwarf standards as no F-type standards were observed during run.
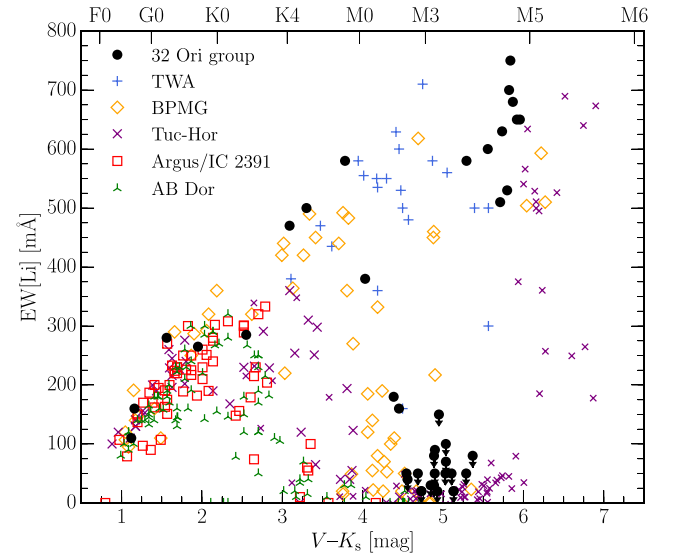^{b}Single F-type standard observed during run.

Figure 7. EW[Li] of newly identified and previously known members of the 32 Ori group as a function of $V - K_s$ colour, compared to other nearby young moving group members compiled from the studies of da Silva et al. (2009), Kraus et al. (2014), Malo et al. (2014) and Binks & Jeffries (2016b). Arrows denote upper limits for which the measured EW[Li] was zero. The depletion pattern closely resembles that of the ∼25 Myr-old β Pictoris moving group (BPMG) and is bracketed by those of the TW Hydrae association (TWA; ∼10 Myr) and Tucana–Horologium (∼45 Myr). The 32 Ori group Li depletion boundary is visible at $V - K_s \approx 5.5$ mag (see Section 5.3).

compared to younger groups. The Li depletion pattern of the 32 Ori group closely mirrors that of the BPMG and is bracketed by those of the TW Hydrae association (TWA) and Tuc-Hor (ages ∼10 and 45 Myr, respectively). In TWA, there are a significant number of Li-rich early-M dwarfs that are clearly absent in the 32 Ori group, for which the Li depletion pattern appears to turn over at a spectral type of ∼M0. Likewise, there are several Li-rich mid to late K-type
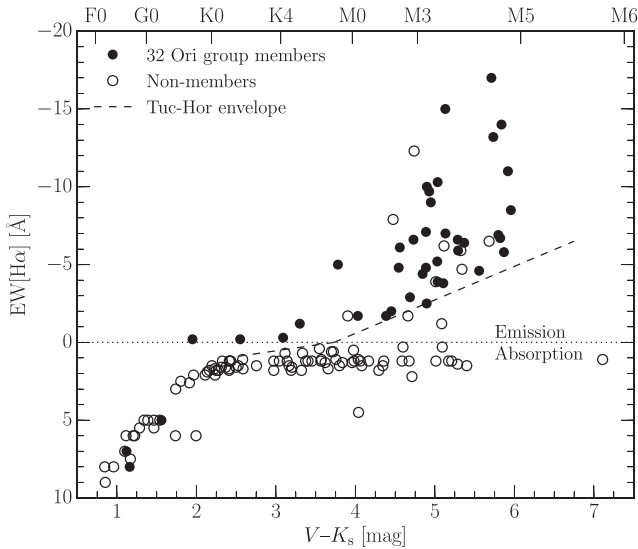
Figure 8. EW[Hα] of all observed candidates and known members of the 32 Ori group as a function of $V - K_s$ colour. At late-G spectral types and beyond, there is a clear distinction between confirmed 32 Ori group members and spectroscopic non-members, whereas at earlier spectral types both show similar levels of Hα absorption. The dashed line denotes the lower envelope of Hα emission from members of the ~45 Myr-old Tucana–Horologium association (Kraus et al. 2014).

Figure 9. Radial velocity residual ($\Delta_{RV} = RV - RV_{expt}$) of all observed candidates and known members of the 32 Ori group as a function of $V - K_s$ colour. The shaded region represents our $|\Delta_{RV}| \leq 5\,\mathrm{km\,s^{-1}}$ membership criterion. Although three stars appear to lie just outside this region, after considering their velocity uncertainties they can be considered members.

stars in the 32 Ori group that are not observed in the older Tuc–Hor (turnover at ~K4). This already provides a relative age ranking, suggesting that the 32 Ori group is older than TWA, younger than Tuc–Hor and approximately coeval with the BPMG (age ~25 Myr).

Given that young moving groups typically have very small intrinsic velocity dispersions ($\sigma_{1D} \lesssim 1.5\,\mathrm{km\,s^{-1}}$; see Mamajek 2016), we would expect the observed radial velocity of a genuine 32 Ori group member to be similar to the line-of-sight projection of the group space velocity at that position (see Section 2.1). We therefore retained only those candidates for which $|\Delta_{RV}| = |RV - RV_{expt}| \leq 5\,\mathrm{km\,s^{-1}}$, after allowing for the uncertainty on the WiFeS velocity (see Binks & Jeffries 2016b). When more than one velocity measurement was made, we adopted the unweighted average and standard deviation (also see discussion in Section 3.2.1). Fig. 9 shows the difference in radial velocity Δ_{RV} for all observed candidates and known members of the 32 Ori group as a function of $V - K_s$ colour. Only three stars have WiFeS velocities that place them just outside the Δ_{RV} limit (all have $|\Delta_{RV}| < 6\,\mathrm{km\,s^{-1}}$; see Table 3). After considering their velocity uncertainties, however, they can all be considered genuine members. One is the known member and SB2 system V1874 Ori ($\Delta_{RV} = 5.3\,\mathrm{km\,s^{-1}}$) that has a high-resolution systemic velocity of $18.4 \pm 0.3\,\mathrm{km\,s^{-1}}$ (see Table 1), giving $\Delta_{RV} = 1.3\,\mathrm{km\,s^{-1}}$. The remaining two stars are both new members, one of which (2M0522+0502) is a possible fast rotator with a broad CCF.

Combining the Li absorption, Hα emission and radial velocity criteria, we identify 28 new members of the 32 Ori group. These new members, all with spectral types between M1.5 and M5.5, are listed in Table 3 along with the 90 non-members and six interesting systems requiring further study (see Section 4.4). The penultimate set of columns in Table 3 list the results of the membership tests described above, with the final membership decision including the proper motion match Δ_{PM} and (kinematic) distance. For convenience, each member is identified by both its 2MASS designation and a shorter 32 Ori group membership number prefixed by the
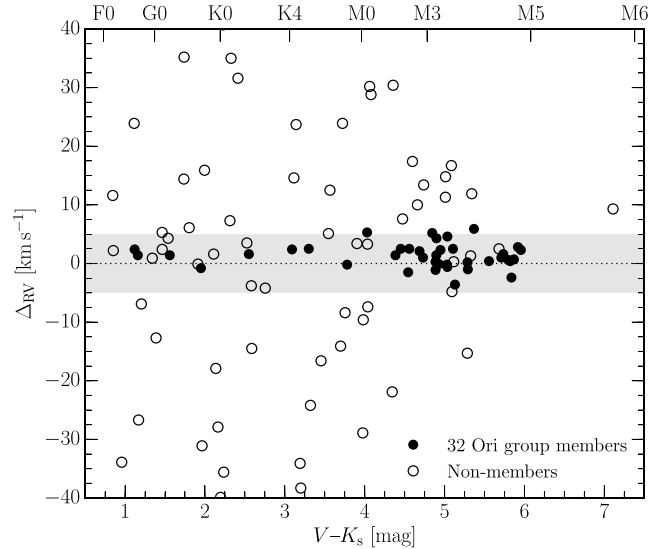
letters THOR, similar to the TWA (TW Hydrae association) and RECX (η Chamaeleontis cluster) nomenclatures commonly used in the literature for other young groups.

4.2 Recently proposed members from the literature

Burgasser et al. (2016) recently proposed the free-floating low surface gravity L1 brown dwarf *WISE* J052857.68+090104.4 as the first substellar member of the 32 Ori group. It is only $3°$ from 32 Ori itself and its estimated distance, proper motion, radial velocity and spectral characteristics are all consistent with group membership. At an age of ~25 Myr, its 1880 K effective temperature implies a mass ($M = 14^{+4}_{-3}\,M_{Jup}$) that straddles the brown dwarf/planetary-mass boundary.

Riedel et al. (2016) also proposed the Li-poor M2.5 star SCR 0522−0606 (2MASS J05224069−0606238) as a potential 32 Ori group member on the basis of its proper motion, spatial position and low surface gravity. Their SALT/RSS radial velocity of $-1.5 \pm 5.0\,\mathrm{km\,s^{-1}}$, however, is approximately 4σ from the ~21 km s^{-1} expected of a genuine member at that position. To test for spectroscopic binary, we obtained WiFeS/$R7000$ spectra on 2016 October 14 and 2017 January 7, finding a mean radial velocity of $25.6 \pm 1.9\,\mathrm{km\,s^{-1}}$ and a spectral type of M3. The spectra showed broad, unresolved CCFs (FWHM = 3.6 px) and double-peaked He I 5876 Å emission lines, both suggestive of binary. The star is outside our $10°$ survey radius, but based on its UCAC4 proper motion, we calculate $\Delta_{PM} = 7.9\,\mathrm{mas\,yr^{-1}}$ at $d_{kin} = 88$ pc. At this distance, SCR 0522−0606 has $M_V = 9.55$ mag and an elevated CMD position consistent with an equal-mass binary. Given its low gravity, distance, radial velocity and reasonable proper motion, we confirm membership of SCR 0522−0606 in the 32 Ori group.

Including these two objects (as well as HD 36002, see Section 4.3.1), there are currently 46 known 32 Ori group members. Note that given the limited areal coverage and depth of this study, the true stellar census of the group is almost certainly
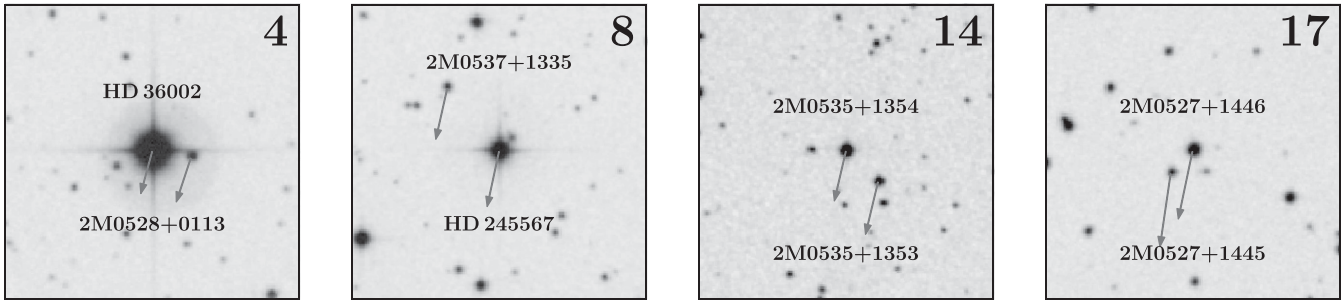
Figure 10. Red Digitized Sky Survey images of the four wide pairs confirmed as members of the 32 Ori group during this study (the large number in the upper right corner of each image corresponds to the THOR number assigned as part of this study; see Table 3). Each image is 3×3 arcmin and oriented north up, east left. Arrows show the UCAC4 proper motions projected over a period of 1000 yr. Each pair clearly shares a common proper motion in addition to a common distance and radial velocity. From left to right, their physical separations are approximately 2600, 5500, 3000 and 1600 au.

incomplete (especially at lower masses) and this number should be treated as a lower limit.

4.3 Notable systems

4.3.1 *2MASS J05284050+0113333 (THOR 4B)*

2M0528+0113 (M3.5, $d_{kin} = 99$ pc) is only 24 arcsec from and co-moving with the early-type star HD 36002 (see Fig. 10), which was in our final candidate list ($d_{kin} = 105$ pc, $\Delta_{PM} = 0.2$ mas yr^{-1}) but not initially observed. It was, however, observed by both *Hipparcos* ($d = 103^{+9}_{-8}$ pc; van Leeuwen 2007) and *Gaia* (112^{+8}_{-7} pc; including the additional ± 0.3 mas systematic uncertainty on the parallax as described in Gaia Collaboration et al. 2016). Its *Gaia* DR1 proper motion is <2 mas yr^{-1} from that expected of a 32 Ori group member at the weighted mean distance of 109^{+6}_{-5} pc and 2M0528+0113 is <3 mas yr^{-1} discrepant, well within its 5.8 mas yr^{-1} URAT1 uncertainties. We obtained two WiFeS R7000 spectra of HD 36002 on 2017 January 11 and find it to be an SB2 system (see Table 5) with an estimated spectral type of A7. Given their close separation, congruent distances and proper motions, we propose HD 36002 and 2M0528+0113 are a genuine comoving pair separated by $\sim$2600 au and thus HD 36002 is also a member of the 32 Ori group (THOR 4A; see Table 3).

4.3.2 *2MASS J05372061+1335310 (THOR 8B)*

This M3 star is 50 arcsec north-east of the previously known G5 member HD 245567 (THOR 8A; see Fig. 10). At a kinematic distance of 113 pc, 2M0537+1335 has a space motion only 1.5 km s^{-1} from the mean 32 Ori group velocity. HD 245567 has a kinematic distance of 104 pc, which agrees with that of 2M0537+1335 (physical separation of $\sim$5500 au) to within the uncertainties propagated from their respective proper motions. Neither star has a *Hipparcos* or *Gaia* DR1 parallax. A wider possible comoving companion, the M5.5 2MASS J05373000+1329344, is 6 arcmin from HD 245567 at a distance of 110 pc, corresponding to a separation of $\sim$40 kau.

4.3.3 *2MASS J05351761+1354180 (THOR 14A)*

This new Li-rich M1.5 member is only 27 arcsec from 2MASS J05351625+1353594 (THOR 14B, M3.5; see Fig. 10). The *ROSAT* source 1RXS J053516.6+135404 is more likely associated with the lower mass component. Despite observed radial velocities 3–5 km s^{-1} larger than expected (noting that 2M0535+1354 is a

suspected SB1; see Table 4), both stars are excellent proper motion matches to the group ($\Delta_{PM} < 2$ mas yr^{-1}) at distances of 116 and 110 pc, respectively, and are unequivocal members of 32 Ori with a separation of $\sim$3000 au.

4.3.4 *2MASS J05274313+1446121 (=DIL7; THOR 17A)*

2M0527+1446 (spectral type M3) is associated with the *ROSAT* source 1RXS J052743.4+144609 and was catalogued as an Hα emission line object (DIL7) in the north-western outskirts of the λ Orionis star-forming region by Duerr, Imhoff & Lada (1982). It forms a 19 arcsec wide pair with the M5 member 2MASS J05274404+1445584 (THOR 17B; see Fig. 10). Both stars are excellent kinematic matches to the mean 32 Ori group space motion ($\Delta_{UVW} < 2$ km s^{-1}) at inferred distances of 87 and 82 pc, respectively. At such distances, their angular separation corresponds to $\sim$1600 au. The pair are unlikely to be λ Orionis members, given both the much larger distance to the association and its significantly younger age ($\sim$400 pc and $\sim$10 Myr, respectively; see Bell et al. 2013), and thus, we assign them as members of the 32 Ori group. Interestingly, both this pair and THOR 14AB have components either side of the 32 Ori group lithium depletion zone but in the opposite sense; THOR 17A (M3) and THOR 14B (M3.5) lie in the Li-poor region, while THOR 17B (M5; EW[Li] = 580 mÅ) and THOR 14A (M1.5; 180 mÅ) are Li-rich. Component identifications and Washington Double Star (WDS) catalogue parameters for these four new wide systems are listed in Table 6.

4.3.5 *2MASS J05363692+1300369 (THOR 31)*

The 2016 January 25 spectrum of this Li-rich SB2 member (combined spectral type M4.5) showed a strong (EW ≈ -5 Å) emission line $\sim$400 km s^{-1} redwards of Hα, near the rest wavelength of 6573 Å Ca I (see Fig. 11). Inspection of the raw image shows that the emission is associated with a single source and not the sky background or extended nebular emission. The feature is clearly variable as only Ca I absorption is seen in two 2016 October observations a night apart, but a weaker emission 'bump' at +200 km s^{-1} is visible in the 2017 January 7 spectrum. At all times, the shape and strength of Hα remained approximately constant. The emission features cannot be red-shifted Hα from the companion, whose velocity offset is only $\sim$50 km s^{-1} based on the broad but unresolved CCF and double-peaked Hα line.

Given the lack of excess Hα, other Ca emission lines (e.g. Ca I 6717 Å) or any emission lines in the January spectrum typically

Table 6. Wide binaries discovered in this study. Column 1 lists the THOR number for each component as assigned in this study, whereas column 3 provides the Washington Double Star (WDS) catalogue designation assigned based on the position of the primary.

THOR no.	Component designation	WDS designation	Epoch (Ref.) (yr)	PA (°)	Sep. (arcsec)	V (mag)
4A	HD 36002	05287+0113	2000.08 (2MASS)	261.46	24.01	7.46
4B	2MASS J05284050+0113333		2015.00 (*Gaia*)	261.16	24.01	14.74
8A[a]	HD 245567	05373+1335	1998.74 (2MASS)	39.46	49.79	9.54
8B[b]	2MASS J05372061+1335310		2015.00 (*Gaia*)	39.47	49.82	14.96
14A	2MASS J05351761+1354180	05353+1354	1998.74 (2MASS)	226.71	27.12	13.53
14B	2MASS J05351625+1353594		2015.00 (*Gaia*)	226.07	27.27	14.95
17A	2MASS J05274313+1446121	05277+1446	1998.73 (2MASS)	135.95	18.98	14.13
17B	2MASS J05274404+1445584		2015.00 (*Gaia*)	135.05	18.95	16.26

[a]HD 245567 is itself a 0.3 arcsec close binary (see Metchev & Hillenbrand 2009) with the WDS catalogue labelling the components Aa and Ab.
[b]The WDS catalogue lists four additional components to HD 245567 (labelled B–E) with separations of between ∼3 and 11 arcsec; however, astrometry indicates that these companions are unphysical (see Metchev & Hillenbrand 2009). We therefore simply adopt the label B for 2M0537+1335.
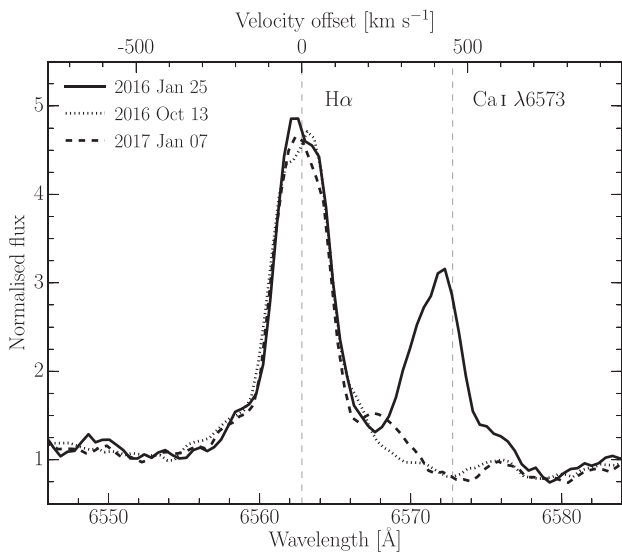
Figure 11. Multi-epoch Hα-region spectra of 2MASS J05363692+1300369 (THOR 31) showing the strong emission feature ∼400 km s^{-1} redwards of Hα. All spectra have been shifted to the heliocentric rest frame, with the rest wavelengths of Hα and Ca I at 6573 Å, given by the dashed lines. Note the double-peaked (SB2) structure of the Hα emission.

associated with flare activity (especially He I 5876 and 6678 Å), we do not believe this line is associated with flare-driven Ca I 6573 Å. Instead, we propose it is red-shifted Hα emission arising from an eruptive prominence or coronal mass ejection (CME) moving away from the system at close to its escape velocity (c.f. ∼350 km s^{-1} for $M = 0.1\,M_\odot$ and $R = 0.3\,R_\odot$, appropriate for a 25 Myr star of $T_{\rm eff} = 3000$ K; Baraffe et al. 2015). Balmer line emission from CMEs has been detected in a handful of active M dwarfs (e.g. Houdebine, Foing & Rodono 1990; Guenther & Emerson 1997; Fuhrmeister & Schmitt 2004) but is typically associated with con-temporaneous flare activity and a *blueshifted* asymmetry in the line profile. That we observed redshifted emission with a projected ve-locity of 400 km s^{-1} outside of an obvious flare event suggests the ejected material was long-lived and large enough to not be com-pletely occulted by the stellar disc. The role of the binary companion in this scenario also remains unclear. High-cadence monitoring of 2M0536+1300 would be useful to firmly establish the nature of the January 25 emission and the frequency of such events.

4.4 Potential members requiring further study

Below we present notes on six systems that we have assigned a mem-bership of '?' in Table 3 (provided in full as Supporting Information with the online version of the paper). Improved spectroscopic, as-trometric or photometric data is required to unequivocally assign membership of these stars to the 32 Ori group.

4.4.1 2MASS J05525572−0044266

2M0552−0044 was classified as a detached, Algol-type eclipsing binary with a period of 0.86 d by the Catalina Sky Survey (CSS; Drake et al. 2014), and as such makes it a rare example of an eclips-ing M dwarf (unresolved spectral type M3). Its phased $V_{\rm CSS}$ light curve is plotted in the top panel of Fig. 12. We confirm binarity from two radial velocities of +65.5 and −39.3 km s^{-1} ($\Delta t = 357$ d, see Table 5) and a variable, double-peaked Hα emission line. We ob-tained five more WiFeS observations of the star during 2017 January 7–9 for the purposes of establishing a preliminary orbital solution. Although the secondary component was not visible in the CCF, we estimated its velocity at each epoch by measuring the velocity offset between Hα peaks and adding this to the primary velocity derived from cross-correlation. One observation did not show a double Hα line, implying its radial velocity (18.4 km s^{-1}) is close to systemic. Using these velocities, we fit Keplerian orbits of period 0.8589884 d (Drake et al. 2014) using standard least squares methods and derive the solution listed in Table 7 and the middle panel of Fig. 12. The system has a total mass of $(M_1 + M_2)\sin^3 i = 0.6\,M_\odot$ and separation $a\sin i = 3.2\,R_\odot$. Assuming $i = 90°$, this corresponds to component masses of approximately 0.44 and 0.16 $M_\odot$. Given the agreement between the fitted systemic velocity of 20.9 ± 2.3 km s^{-1} and the 20.6 km s^{-1} expected of a 32 Ori group member at that position, we consider 2M0552−0044 a highly likely member pending further velocity measurements and improved photometry.

The CSS light curve contains 192 measurements over 7.3 yr and is not well sampled around the eclipses. Rotationally modulated pho-tometric variation due to star-spots appearing and disappearing dur-ing that time also likely contributes to scatter in the regions outside the eclipses. This may affect the period determination and makes deriving temperature ratios and radii problematic. Moreover, the APASS V-band magnitude (15.15 ± 0.06 mag) differs significantly from the CSS photometry. The accuracy of these data is limited by the transformation to $V_{\rm CSS}$ from the unfiltered survey photometry,
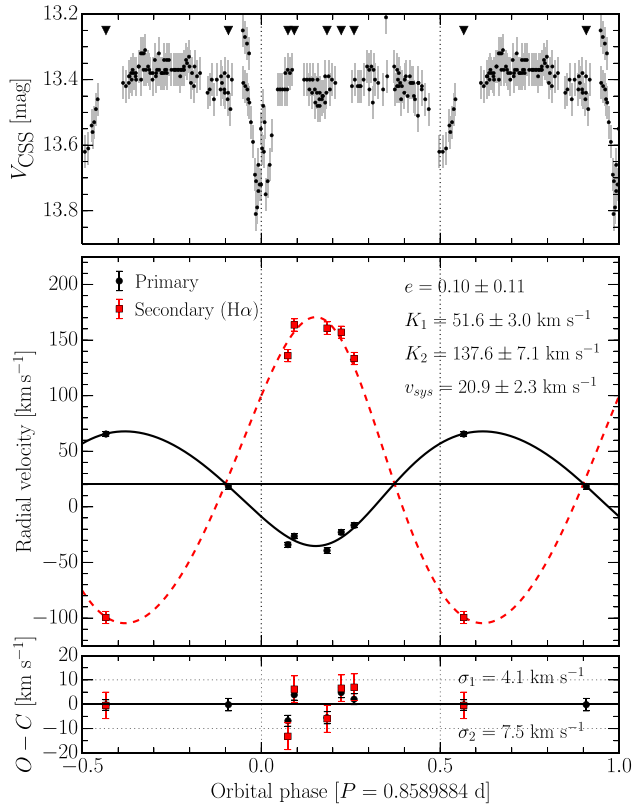
Figure 12. Top: Catalina Sky Survey V_{CSS}-band light curve of the eclipsing binary 2MASS J05525572−0044266. The data have been phased with a period of 0.8589884 d (Drake et al. 2014) and offset such that the primary eclipse occurs at $\phi = 0$. Triangles denote the phases at which the WiFeS spectra were taken. Middle: Keplerian radial velocity curves (see Table 7) fitted to the WiFeS data and phased with the light curve. The derived systemic velocity (20.9 km s^{-1}) is shown by the horizontal line. The large offset from this velocity at zero phase immediately implies a non-zero eccentricity. Bottom: velocity residuals from the best fit. Note that both the secondary velocities and their residuals are correlated with the primary velocities, as expected (see the text).

Table 7. Preliminary orbital and physical parameters of 2MASS J05525572−0044266, derived from a least-squares Keplerian orbit fit to the primary and secondary velocities from Table 5. Uncertainties were propagated from the covariance matrix of the fit. Similar orbital parameters are obtained fitting only the primary velocities.

Period, P	0.858 9884 d (fixed)
Eccentricity, e	0.10 ± 0.11
Primary velocity semi-amplitude, K_1	51.6 ± 3.0 km s^{-1}
Secondary velocity semi-amplitude, K_2	137.6 ± 7.1 km s^{-1}
Systemic velocity, γ	20.9 ± 2.3 km s^{-1}
Epoch of periastron passage (MJD), τ	$57\,319.228 \pm 0.064$
Orientation of periastron, ω	$211 \pm 33°$
Mass ratio, $q = M_2/M_1$	0.375 ± 0.029
Total mass, $(M_1 + M_2)\sin^3 i$	$0.602 \pm 0.074\,M_\odot$
Semimajor axis, $a\sin i$	$0.01494 \pm 0.000\,61$ au
	$3.21 \pm 0.13\,R_\odot$
Assuming inclination $i = 90°$:	
Primary mass, M_1	$0.438 \pm 0.058\,M_\odot$
Secondary mass, M_2	$0.164 \pm 0.019\,M_\odot$

and is only appropriate for the G-dwarf calibrators used by the survey. From 445 Landolt standard stars, Drake et al. (2013) derived $V = V_{CSS} + 0.31(B − V)^2 + 0.04$, which for $(B − V)_{APASS} = 1.51$ yields $V = 14.2$ mag. After re-deriving this relation, we find it is well defined for standards as red as 2M0552−0044, so the remaining discrepancy is likely due to binarity affecting the transformation. We therefore adopt the APASS photometry, which provides a CMD position appropriate for a 25-Myr-old M3 star at ∼90 pc.

We are obtaining high-cadence photometry and further radial velocity observations of the system and will present a full reanalysis and characterization, including final 32 Ori group membership, in an upcoming work. Until then, we note that 2M0552−0044 is Li poor, satisfies both selection criteria ($\Delta_{PM} = 2.5$ mas yr^{-1}, $d_{kin} = 92$ pc), and is likely associated with the X-ray source 1RXS J055257.7−004424.

4.4.2 BD+08 900AB (=HD 34081AB)

A 4 arcsec A7+F2 near-equal brightness binary, BD+08 900AB is resolved in UCAC4 and we obtained spectra for both components during good seeing (1.5 arcsec FWHM) WiFeS observations in 2015 September and 2017 January. BD+08 900B may be an SB2 while the primary is a possible fast rotator (see Section 3.2.1). Both stars have radial velocities that are consistent with 32 Ori group membership at ≲2 km s^{-1} and BD+08 900B is an excellent proper motion match ($\Delta_{PM} = 1.5$ mas yr^{-1}) at a kinematic distance of 82 pc. BD+08 900A's UCAC4 proper motion is significantly smaller and a poor match at any distance. The combined system was observed with *Hipparcos* ($d = 120^{+22}_{-16}$ pc) and *Gaia* (97^{+6}_{-5} pc). Adopting the astrometry of the latter, BD+08 900AB is only 3 km s^{-1} from the 32 Ori group mean space motion and the EW[Li] = 130 mÅ we measure for BD+08 900B is similar to young F-type stars in Fig. 7. Until the binary nature of BD+08 900B is confirmed we refrain from assigning the system to the 32 Ori group, but note it is a strong kinematic candidate.

4.4.3 HD 37825

HD 37825 is a new SB3 system (see Fig. 6) that we observed at four epochs (see Table 4), one of which (2016 February 21) exhibited narrow, single lines and a radial velocity of 28 km s^{-1}, which must be near-systemic. This is in reasonable agreement with the ∼20 km s^{-1} expected of a 32 Ori group member at that position and there is also a moderately good proper motion match to the group ($\Delta_{PM} = 6.8$ mas yr^{-1}) at a kinematic distance of 84 pc. The 2016 October and 2017 January spectra showed clearly resolved double lines with a weaker tertiary component. However, only two components are visible in the CCF, separated by ∼140 km s^{-1}. The system does not have a *Hipparcos* or *Gaia* DR1 parallax or proper motion. The EW[Li] = 130 mÅ we measured in the single-lined spectrum is typical of a young F5 star (see Fig. 7). Higher resolution spectroscopy of the system and a velocity curve would be useful in confirming its membership.

4.4.4 2MASS J05053333+0044034

2M0505+0044 satisfies both UCAC4 selection criteria ($\Delta_{PM} = 5.0$ mas yr^{-1}, $d_{kin} = 90$ pc) and also shows depleted lithium, consistent with its M2.5 spectral type. The star's radial velocity, however, is rather discrepant ($\Delta_{RV} = 13.4$ km s^{-1}). Coupled with a broad Hα line ($\Delta v \approx 300$ km s^{-1} at 10 per cent of peak flux;

EW[Hα] = −12.3 Å) and strong He I 5876 and 6678 Å, Na D and X-ray emission (1RXS J050533.4+004421), this could be indicative of spectroscopic binarity. The star's CCF is not broadened, suggesting it is not a fast rotator or SB2. Choosing to ignore the $|\Delta_{RV}| < 5$ km s^{-1} velocity threshold would have implications for other candidates and so we retain 2M0505+0044 as a possible member requiring further velocity measurements.

4.4.5 2MASS J05561307+0803034

2M0556+0803 easily satisfies both selection criteria ($\Delta_{PM} = 0.5$ mas yr^{-1} and $d_{kin} = 97$ pc), whereas its mean radial velocity is somewhat discrepant ($\Delta_{RV} = 7.6$ km s^{-1}). On its own, this would suggest non-member status, however, the star's CCF is rather broad (FWHM = 3.8 px) and a double-peaked He I 5876 Å emission line suggests SB2 binarity. Furthermore, 2M0556+0803 lies in a region of the CMD surrounded by other Li-depleted group members (to within the uncertainties on its photographic V-band magnitude), consistent with an M4 spectral type. We therefore retain 2M0556+0803 as a possible member to be re-examined when further spectroscopic observations become available.

4.4.6 2MASS J05572121+0502158

2M0557+0502 satisfies the proper motion selection criterion ($\Delta_{PM} = 1.3$ mas yr^{-1}) and at a kinematic distance of 115 pc was one of a small number of distance outliers in our sample observed with WiFeS. The star's radial velocity, however, is strongly inconsistent with membership ($\Delta_{RV} = 30.4$ km s^{-1}). The presence of a strong Li line (EW[Li] = 290 mÅ) suggests 2M0557+0502 is young, but we also find its rising spectrum is significantly reddened [$E(B − V) \approx 0.6$ mag], with an underlying spectral type of K2. This level of reddening is more than an order of magnitude greater than the group mean of $E(B − V) = 0.03$ mag (see Section 5.1). Assuming $(V − K_s)_\circ \approx 2.3$ mag appropriate for an early K-dwarf and a de-reddened $M_V \approx 7.2$ mag at 115 pc, 2M0557+0502 lies 1–2 mag below the 32 Ori group CMD sequence and is unlikely to be a member, especially if it is an SB1. Given the strong reddening and large radial velocity, it could be a Li-rich background giant, but we seek a better spectroscopic characterization before finalizing its evolutionary and membership status.

4.5 Comparison to previous non-spectroscopic surveys

Since its initial discovery by Mamajek (2007), there have been no surveys dedicated *specifically* to discovering new members of the 32 Ori group, with new members being individually added on the basis of common attributes like proper motion and radial velocity (Mace et al. 2009; Franciosini & Sacco 2011). Given that in this work, we aim to characterize the stellar population of the 32 Ori group, it is important that we place our new members in context by re-examining previous non-spectroscopic memberships from large surveys of Galactic open clusters and associations.

As part of their global catalogue of Milky Way clusters, Kharchenko et al. (2013) recovered the 32 Ori group, arguing that it comprises 40 members within a radius of 2°.2, lies at a distance of 95 pc and has an age of 32 Myr. They found a mean proper motion and radial velocity of ($\mu_\alpha \cos \delta, \mu_\delta$) $\simeq$ (10.0, −32.2) mas yr^{-1} ($\sigma_\mu \simeq \pm 0.8$ mas yr^{-1}) and 13.1 km s^{-1}, respectively. Kharchenko et al. (2013) assigned membership probabilities using a combination of three metrics: one kinematic (based on the proper motion of

a given object with respect to the cluster mean) and two photometric (based on positions in the K_s, $J − H$ and $J − K_s$ CMDs). Stars that satisfied all three metrics with a probability greater than 61 per cent were classified as 'most probable' members. Cross-matching their 40 most probable members with the 45 stellar group members of this study, we find only three objects in common: HR 1807, HD 35714 and HD 36338. In other words, the Kharchenko et al. (2013) selection criteria omit 32 Ori as a member of the 32 Ori group! Furthermore, cross-matching their members against potential kinematic members from UCAC4 and URAT1 (see Section 2.1), we find 13 and 40 objects in common, respectively. Aside from HR 1807, HD 35714 and HD 36338, none of the other candidates have CMD positions or Δ_{PM} values consistent with membership in the 32 Ori group.

The main reason the Kharchenko et al. (2013) membership for late-type objects is particularly unreliable is due to their reliance on near-infrared 2MASS CMDs. At low effective temperatures ($T_{eff} \lesssim 4000$ K), isochrones in both the K_s, $J − H$ and $J − K_s$ CMDs become vertical and essentially degenerate with age. This removes any meaningful photometric distance information and means that the study was reliant solely on deeper but less accurate PPMXL proper motions for membership. We note that within their cluster radius of 2°.2 there are 15 new members from Table 3 that could have provided matches. Of these, 13 failed the kinematic test and two failed the photometric tests. Clearly, these tests are too restrictive and the PPMXL proper motions not accurate enough to rely on for membership determinations.

The 32 Ori group is also listed (as Mamajek 3) in the catalogue of optically visible open clusters by Dias et al. (2002, v.2.5; 2005). Recently, Dias et al. (2014) used UCAC4 astrometry to provide membership probabilities for individual stars by fitting the observed proper motion distribution in a region surrounding each cluster with two elliptical bivariate populations. Based on an apparent diameter of 250 arcmin, Dias et al. (2014) identified over 2.8×10^4 UCAC4 counterparts, of which 2.3×10^4 were assigned to the 32 Ori group, making it the twelfth most populous cluster in the entire catalogue. From these members, they estimated a mean group proper motion of ($\mu_\alpha \cos \delta, \mu_\delta$) = (0.55, −2.75) mas yr^{-1}, which is not only inconsistent with our proper motion (see Table 2), but also the proper motion listed in the original Dias et al. (2002) catalogue. Cross-matching our 45 stellar members with the sources identified by Dias et al. (2014), we find only 15 objects in common (11 of which are previously known members, see Table 1; 28 lie outside the adopted diameter of the group). None has a membership probability greater than 69 per cent. As with the Kharchenko et al. (2013) study, 32 Ori itself appears to be a non-member of its own group, making it hard to place much credibility in the Dias et al. (2014) results. Their membership probabilities are based solely on the proper motion of an object relative to the mean, which alone is not sufficient to unambiguously demonstrate membership.

5 PROPERTIES OF THE 32 ORI GROUP

Below we use the previously known and new members of the 32 Ori group to investigate its global properties; namely interstellar reddening, age, circumstellar disc frequency and spatial structure.

5.1 Reddening and extinction

Before attempting to determine an age for the 32 Ori group from its CMD, the effects of interstellar reddening must first be accounted for. The 32 Ori group lies at a distance of ∼90 pc,

Table 8. Reddening estimates for the known B-, A- and F-type members of the 32 Ori group.

THOR no.	Name	$E(B-V)$ (mag)	Method
1AB	32 Ori AB	0.01	Q-method (*UBV*)
1A	32 Ori A	0.01	$B-V$, SpT
1B	32 Ori B	0.06	$B-V$, SpT
2	HR 1807	0.00	Q-method (*UBV*)
2	HR 1807	0.01 ± 0.01	SED (*UBVJHK*$_s$, SpT)
3A	HD 35714	0.05 ± 0.02	SED (*BVJHK*$_s$, SpT)
3B	HD 36823	0.02	$B-V$, SpT
4A	HD 36002	0.03	$B-V$, SpT
5	HD 35499	0.04 ± 0.02	SED (*BVJHK*$_s$, SpT)
6	HD 36338	0.03 ± 0.02	SED (*BVJHK*$_s$, SpT)
7	HD 35695	0.06 ± 0.02	SED (*BVJHK*$_s$, SpT)
	Median	**0.03 ± 0.01**	

and while reddenings for stars at this distance are typically low [$E(B-V) \lesssim 0.05$ mag], the complex shape of the Local Bubble and surrounding clouds is such that the reddening is not necessarily negligible (Reis et al. 2011).

In Table 8, we list $E(B-V)$ estimates for the bright B-, A- and F-type members of the 32 Ori group using the best available spectral types and photometry. For the two B-type members (unresolved 32 Ori and HR 1807), we adopt the *UBV* photometry from Mermilliod (2006) and combine this with the *Q*-method (Pecaut & Mamajek 2013) to derive negligible reddenings of $E(B-V) = 0.01$ and 0.00 mag, respectively. Using resolved *BV* photometry from *Tycho*-2, and adopting spectral types of B5 and B7 for 32 Ori A and B from Edwards (1976), and A7 and A7.5 for HD 36002 and HD 36823, we estimate $E(B-V) = 0.01$, 0.06, 0.03 and 0.02 mag, respectively. For the five other members, we fit the *BVJHK*$_s$ photometry (and for HR 1807, *U* band from Johnson 1966) to the intrinsic dwarf colour locus of Pecaut & Mamajek (2013), calculating χ^2 fits for spectral energy distributions (SEDs) spaced in $T_{\rm eff}$ by 10 K and in steps of $E(B-V) = 0.01$ mag. The quoted $E(B-V)$ values reflect the distribution of those fits for which the χ^2 probability $q > 5$ per cent over the range of $T_{\rm eff}$ reflecting a ±1 subtype uncertainty in spectral type (where B9.5V to A0V was counted as a full step in subtype). The uncertainties in the $E(B-V)$ estimates from the SED fitting are typically ±0.02 mag.

Based on the values in Table 8, we adopt a median reddening towards the group of $E(B-V) = 0.03 \pm 0.01$ mag, which translates to a *V*-band extinction of $A_V = 0.10 \pm 0.03$ mag and a K_s-band extinction of $A_{K_s} = 0.011 \pm 0.004$ mag (following Bilir et al. 2008). The range of values [$E(B-V) \lesssim 0.06$ mag] are suggestive of small amounts of patchy extinction across the core of the group. Note that the K_s-band extinction is smaller than the typical 2MASS photometric errors.

5.2 Isochronal age

Fig. 13 shows the M_V, $V-K_s$ CMD of the 45 stellar members of the 32 Ori group. We preferentially use trigonometric parallaxes to transform the apparent *V*-band magnitudes listed in Table 3 to M_V; however, in the majority of cases, these are not available and so we adopt the kinematic distances from our selection process (see Section 2.1). Note that for parallaxes from the recent *Gaia* DR1, we include the additional systematic uncertainty of ±0.3 mas as discussed in Gaia Collaboration et al. (2016). Our adoption of the best-fitting kinematic distances is in contrast to Bell et al. (2015) in

which we simply adopted the mean group distance for the 11 stars listed in Table 1 without parallaxes (barring HD 36823 that was not included in that study), and has resulted in a less tight colour–magnitude sequence in Fig. 13. Uncertainties on M_V incorporate the uncertainties in the proper motions used to calculate the kinematic distances (typically several mas yr^{-1}) and result in distance uncertainties in the range of 8–30 per cent.

We derive an isochronal age for the 32 Ori group using the same method as that described in previous papers (see e.g. Bell et al. 2014; Bell et al. 2015), namely by fitting two-dimensional probability distributions to the CMD using the τ^2 fitting statistic of Naylor & Jeffries (2006) and Naylor (2009). In brief, the probability distributions are created using stellar evolutionary models and not only include binarity but also incorporate an empirical colour–$T_{\rm eff}$ relation and bolometric corrections from observations of low-mass Pleiades members, as well as theoretical corrections for the dependence on surface gravity. For our isochronal age analysis, we have adopted the following interior models: Dartmouth (Dotter et al. 2008), PARSEC (Bressan et al. 2012), BHAC15 (Baraffe et al. 2015) and Pisa (Tognelli, Prada Moroni & Degl'Innocenti 2015). Note that the Pisa models are based on the same calculations as described in Tognelli et al. (2015); however, they cover a mass range of $0.08 < M/M_\odot < 9$. As per Section 5.1, we have included the effects of interstellar reddening, adopting a group mean $E(B-V) = 0.03$ mag. Table 9 lists the individual isochronal ages for the 32 Ori group in addition to our mean isochronal age of 25 ± 5 Myr (±4 Myr statistical, ±3 Myr systematic).

5.3 LDB age

The LDB is defined as the sharp transition between stars that have contracted sufficiently that their core temperatures have reached the critical value to burn Li and thus exhibit depleted levels of Li in their photospheres, and those stars at slightly lower masses that have not yet reached this critical temperature and show undepleted levels. Over the past few years, the LDB has been extolled as the least model-dependent, absolute age-dating technique for coeval populations with ages of between ∼20 and 200 Myr (see e.g. Soderblom et al. 2014).

As shown in Fig. 13, the LDB in the 32 Ori group is defined by the Li-poor M4.5 member 2MASS J05313290+0556597 (THOR 30) and the Li-rich (EW[Li] = 600 mÅ) M4.5 member 2MASS J05264073+0712255 (THOR 32). We note that neither of these stars appear to be an unresolved binary that could significantly affect the determination of the LDB luminosity. To derive an LDB age for the group, we adopt the method described in Binks & Jeffries (2014, 2016b), which involves defining a region in the CMD at which the LDB is located and then fitting curves of constant luminosity corresponding to 99 per cent Li depletion. These curves are created using stellar evolutionary models after transforming $L_{\rm bol}$ and $T_{\rm eff}$ to absolute *V*-band magnitude and $V-K_s$ colour using the pre-MS bolometric correction and colour relations of Pecaut & Mamajek (2013). Our threshold for Li-poor stars (EW[Li] < 100 mÅ) ensures that, in comparison to the Li-rich stars that exhibit undepleted levels of Li consistent with measurements of young stars at birth (see e.g. Palla et al. 2007), the difference in depletion between the Li-poor and Li-rich stars is greater than a factor of 100, and so calculating the LDB age in such a manner is entirely justified (see also Jeffries & Oliveira 2005; Tognelli et al. 2015).

To define the LDB region, we simply adopt the central position between the two stars and the separation in both colour and magnitude, yielding $V-K_s = 5.462 \pm 0.094$ and
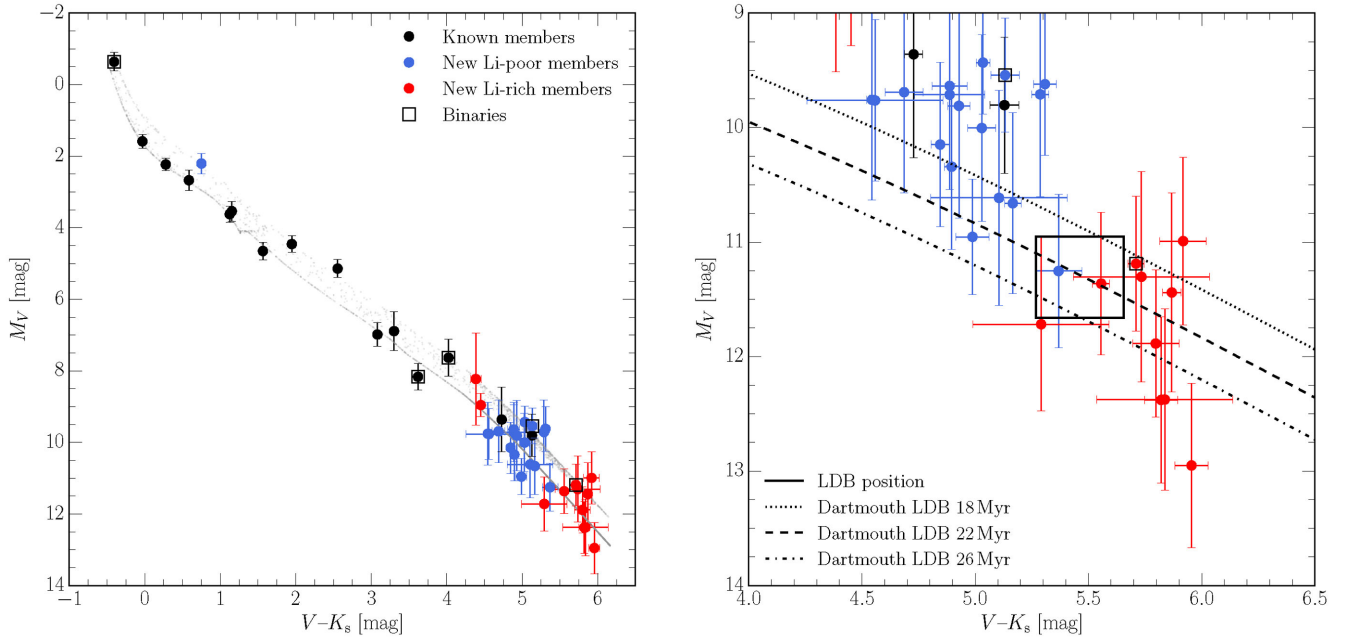
Figure 13. Left: example best-fitting M_V, $V - K_s$ CMD of the 32 Ori group with the Dartmouth models overlaid. The grey points represent individual stars in our two-dimensional probability distribution (see the text) from which we derive a best-fitting age of 23 Myr. The LDB is clearly identified at $V - K_s \simeq 5.5$ mag (spectral type M4.5). Right: the position of the 32 Ori group LDB as defined in this study (see the text). Overlaid are several lines corresponding to loci of constant luminosity at which Li is depleted at the 99 per cent level as predicted by the Dartmouth evolutionary models. The best-fitting LDB age of 22 Myr in this panel is in excellent agreement with the isochronal age based on the same stellar evolutionary models.

Table 9. Isochronal and LDB ages for the 32 Ori group.

Method	Model	Age (Myr)	Mean age (Myr)
Isochrone	Dartmouth	23^{+7}_{-3}	
	BHAC15	28^{+3}_{-4}	$25 \pm 5\,(1\sigma)$
	Pisa	20^{+4}_{-1}	[± 4 (statistical), ± 3 (systematic)]
	PARSEC	29 ± 3	
LDB	Dartmouth	22^{+4}_{-3}	
	BHAC15	22^{+4}_{-3}	$23 \pm 4\,(1\sigma)$
	Pisa	21 ± 3	[± 4 (statistical), ± 1 (systematic)]
	Dartmouth ($\langle Bf \rangle = 2.5$ kG)	26 ± 4	
Final adopted age		**$24 \pm 4\,(1\sigma)$**	
		[± 4 **(statistical)**, ± 2 **(systematic)**]	

$M_V = 11.308 \pm 0.055$ mag. These values are consistent with those reported by Binks & Jeffries (2014) for the BPMG. The LDB age is then calculated by fitting the Li depletion curves to this point and the uncertainty on the age calculated from the size of the region in both colour and magnitude. Note that we have also included an additional uncertainty of 0.1 mag in colour and 0.3 mag in M_V to reflect likely uncertainties in both the photometric calibration (especially the inhomogeneous V-band photometry) and kinematic distances. Table 9 lists the individual LDB ages derived from the following sets of evolutionary models: Dartmouth (including a new prescription for magnetic fields, $\langle Bf \rangle = 2.5$ kG; Feiden & Chaboyer 2013, 2014), BHAC15 and Pisa, which together yield a mean LDB age of 23 ± 4 Myr (± 4 Myr statistical, ± 1 Myr systematic). The individual LDB ages from the non-magnetic Dartmouth, BHAC15 and Pisa models all agree to within 1 Myr, whereas the magnetic Dartmouth models imply an older, yet consistent, age for the group. These findings are similar to those reported by Malo et al. (2014) and Binks & Jeffries (2016b) for the BPMG.

5.4 Final adopted age

The age analyses above clearly demonstrate that the isochronal and LDB ages for the 32 Ori group are in agreement. Combining these two age determinations, we calculate a final adopted age of 24 ± 4 Myr (± 4 Myr statistical, ± 2 Myr systematic). We note that this age is essentially identical to the 23 ± 3 Myr age for the BPMG derived by Mamajek & Bell (2014). The uncertainty in our final adopted age is driven by the statistical uncertainty that stems from (i) the reasonably large uncertainties on the kinematic distances and (ii) the inhomogeneous V-band photometry collated from the available literature. Both of these points will be directly addressed by *Gaia* data releases in the coming years, by providing parallaxes and well-calibrated, homogeneous G-band photometry for all members of the group. This will naturally lead to a tighter sequence in the CMD compared to that shown in Fig. 13 and will allow more statistically robust age determinations.

5.5 Circumstellar disc frequency

Given that the 32 Ori group appears to be essentially coeval with the BPMG, which is known to harbour several optically thin debris discs (e.g. β Pic itself, 51 Eri and AU Mic), it is conceivable that such discs may also be present in the 32 Ori group. These could present ideal targets for direct imaging in an attempt to discover gas giant planets and further constrain potential planetary formation mechanisms. As discussed in the 'Introduction', the *Spitzer* IRAC and MIPS survey described by Shvonski et al. (2016) demonstrates that 4/14 members (not including HD 36823) exhibit 24 μm excess emission, and hence these stars are likely debris disc candidates. In this section, we search for further evidence of circumstellar material around the combined 32 Ori group census.

To identify potential circumstellar discs, we cross-matched our membership against the All*WISE* catalogue (Cutri et al. 2014). All 45 stars have counterparts in the $W1$ (3.4 μm), $W2$ (4.5 μm) and $W3$ (12 μm) bands; however, only 19 were detected in the $W4$ (22 μm) band. Fig. 14 plots the $K_s - W1$, $K_s - W2$, $K_s - W3$ and $K_s - W4$ infrared colours as a function of spectral type for our 32 Ori group members. To determine whether a given star exhibits an infrared excess, we use the pre-MS colour sequence of Pecaut & Mamajek (2013), which essentially defines photospheric colours for stars with ages of $\simeq 5$–40 Myr. Due to a combination of saturation effects and a paucity of early-type stars within the Local Bubble, the Pecaut & Mamajek (2013) photospheric colours only cover spectral types of F0 and later in the *WISE* bandpasses. For earlier spectral types, we adopted the ATLAS9 ODFNEW synthetic colour indices as calculated by Pecaut & Mamajek, which are based on the atmospheric models of Castelli & Kurucz (2004) and for which we assumed $\log g = 4.5$ dex, and interpolated within these for the T_{eff} corresponding to the specific spectral type as prescribed by the dwarf spectral type–T_{eff} relation of Pecaut & Mamajek. We define an excess in a given *WISE* band as any object that lies greater than 3σ above the Pecaut & Mamajek relation, where σ is the photometric uncertainty on the observed colour. We stipulate, however, that for a source to be labelled an excess object, it must also exhibit excesses in each of the longer wavelength *WISE* bandpasses.

The terminology of circumstellar discs can vary depending on which criteria one adopts, thus making like-for-like comparisons between different regions problematic. We therefore adopt the observational criteria described in Luhman & Mamajek (2012) that has been used in several recent studies of nearby young moving groups and associations (see e.g. Kraus et al. 2014; Pecaut & Mamajek 2016). Following Luhman & Mamajek (2012), we can eliminate any full, transitional or evolved discs that all require an excess of $E(K_s - W4) > 3.2$ mag, yielding a disc fraction of <3.9 per cent (68 per cent confidence level) for such discs. Debris discs are classified as objects with excesses of $E(K_s - W4) < 3.2$ mag, which comfortably covers all of the excess objects identified in the bottom-right panel of Fig. 14. Of the 19 objects with $W4$ detections, we identify six – HR 1807 (THOR 2), 2MASS J05284050+0113333 (THOR 4B), HD 36338 (THOR 6), 2MASS J05274313+1446121 (THOR 17A), 2MASS J05274855+0645459 (THOR 27) and 2MASS J05243009+0640349 (THOR 38) – as exhibiting excess emission and derive a debris disc fraction of 32^{+12}_{-8} per cent based on binomial statistics (see Cameron 2011). Of these six stars, THOR 2, 17A and 38 also display varying degrees of excess $W3$ emission. The mid-infrared All*WISE* photometry and excesses for these debris disc candidates are listed in Table 10. In Fig. 15, we show the SEDs for these objects, created from a combination of optical, near- and mid-IR photometric data

including *Tycho*-2 (BV_T), APASS DR9 $BVgri$, 2MASS JHK_s and All*WISE* $W1$–$W4$. Using the Virtual Observatory SED Analyser (VOSA; Bayo et al. 2008), we fitted the observed SEDs with the solar-metallicity BT-Settl CIFIST atmospheric models of Allard, Homeier & Freytag (2011), computed adopting the revised solar abundances of Caffau et al. (2011). Note that due to the upper limit of 7000 K on the CIFIST models, in the case of HR 1807, we instead used the ATLAS9 ODFNEW models of Castelli & Kurucz (2004).

The obvious data set against which to compare our census of circumstellar discs is the recently published *Spitzer* survey by Shvonski et al. (2016). Our *WISE* analysis corroborates that of Shvonski et al. (2016) with neither study finding evidence for the presence of full or warm dusty discs based on a lack of excess detections in all four IRAC bands as well as the *WISE* $W1$ and $W2$ bands. Of the four debris disc candidates identified by Shvonski et al. (2016), we find that both HR 1807 (THOR 2) and HD 36338 (THOR 6) are 22 μm excess sources; however, we do not detect any excess emission from either HD 35499 (THOR 5) or TYC 112-1486-1 (THOR 10), despite Shvonski et al. (2016) determining both exhibit 24 μm emission at $>4\sigma$ above typical photospheric values. The cause of this discrepancy is unclear as neither object is flagged as variable in the All*WISE* catalogue (but see Melis et al. 2012) and visual inspection of the co-added images suggest nothing unusual (e.g. nearby sources, non-uniform background). In the case of TYC 112-1486-1, this could be a sensitivity issue as the signal-to-noise ratio of the $W4$-band measurement is only ~ 3. The remaining four debris disc candidates identified in this study are all new members and thus were not included in the Shvonski et al. (2016) study.

Of the six objects identified as exhibiting $W4$ excesses, the four M dwarf debris disc candidates are of particular note. Studies have demonstrated that as stellar mass decreases, so does the fraction of associated debris discs (see e.g. Lestrade et al. 2009). To date, only three M dwarf debris discs have been confirmed via scattered light observations, all with ages similar to or younger than the 32 Ori group (AU Mic, TWA 7 and TWA 25; see Choquet et al. 2016). If the new debris disc candidates presented in this study (as well as those in the BPMG; see Binks & Jeffries 2016a[5]) can be confirmed by ancillary mid- and far-IR observations, then these would not only represent some of the oldest and lowest-mass stars with such discs, but they would also provide ideal targets for follow-up direct imaging that may help to enhance our understanding of the processes governing the production and dynamics of dust and planetesimals in such systems during an epoch that is believed to be important for terrestrial planet formation.

Fig. 16 shows the debris disc fraction of the 32 Ori group compared to other nearby young groups/associations and clusters (based on excess emission at either 22 or 24 μm). The disc fractions for all other regions have been taken from the compilation of Zuckerman et al. (2012) and the uncertainties calculated as above using

---

[5] Recently, Silverberg et al. (2016) claimed to have identified an M dwarf debris disc candidate (*WISE* J080822.18-644357.3) in the 45-Myr-old Carina association. Their membership is based solely on the SPM4 proper motion, which when combined with the BANYAN II Bayesian membership tool (Gagné et al. 2014), provides a membership probability of 93.9 per cent. Given this reliance on a single observable, it is therefore perturbing to note that the PPMXL μ_δ value differs from that provided by SPM4 by $\simeq 19$ mas yr^{-1}. Prior to confirming membership, we await an improved proper motion and spectroscopic observations of the star, most importantly a radial velocity in agreement with the ~ 21 km s^{-1} expected of a Carina member at that position.
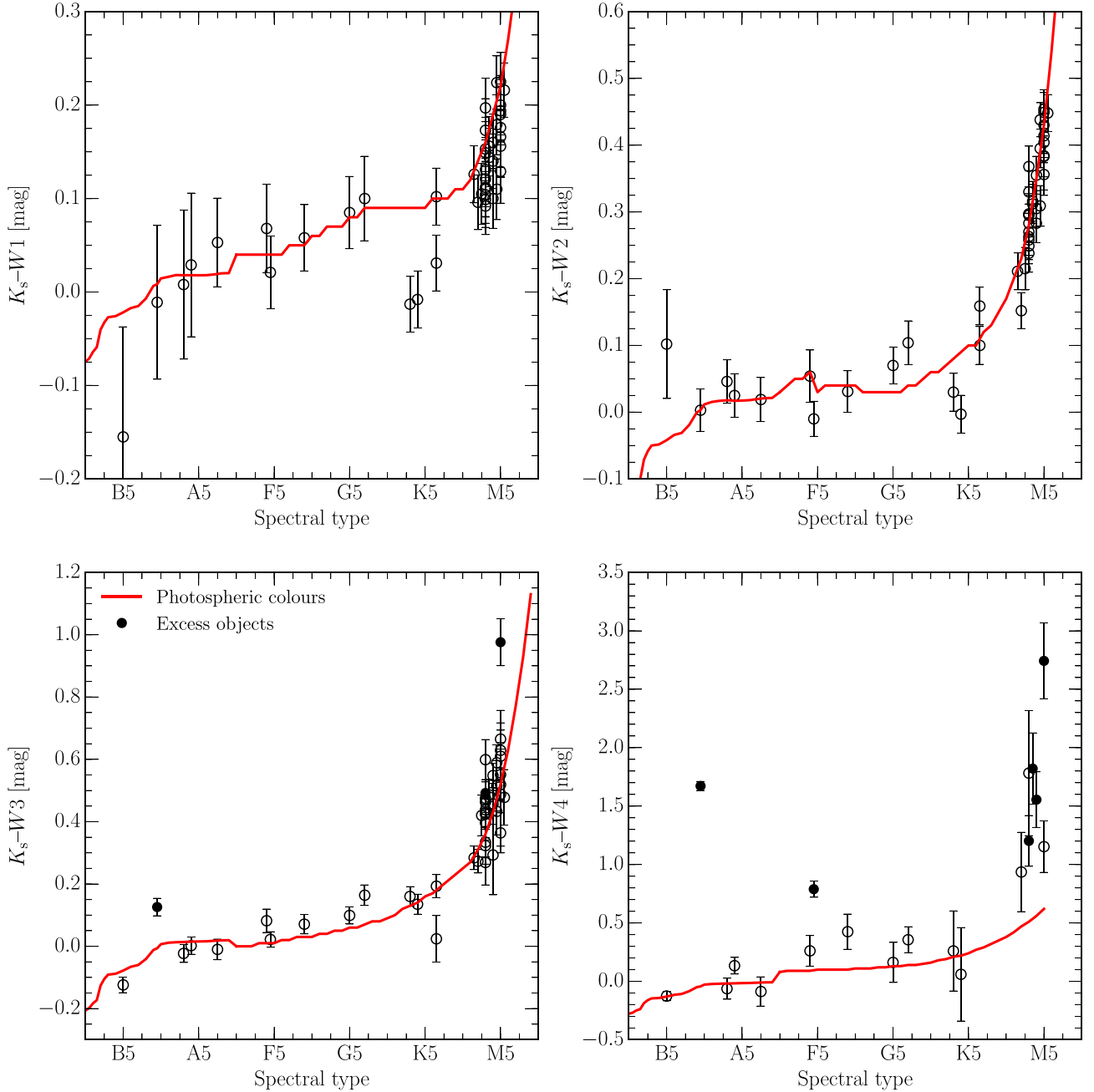
Figure 14. $K_s - W1$, $K_s - W2$, $K_s - W3$ and $K_s - W4$ infrared colours as a function of spectral type for the 45 stellar members of the 32 Ori group (only 19 of which have detections in the $W4$ bandpass). The solid line in each panel represents the expected intrinsic photospheric colours. For spectral types later than F0, these are taken from the pre-MS relations provided by Pecaut & Mamajek (2013), whereas for earlier spectral types, these are based on the synthetic colours from the ATLAS9 ODFNEW atmospheric models of Castelli & Kurucz (2004). Objects deemed to have an infrared excess arising from circumstellar material must lie 3σ above the photospheric colours in a given bandpass as well as every other bandpass at longer wavelengths. Six stars are identified as exhibiting excess $W4$ emission, three of which also demonstrate $W3$ excesses.

Table 10. Mid-infrared photometry and excesses for 32 Ori group debris disc candidates.

THOR no.	WISE J designation	W1 (mag)	W2 (mag)	W3 (mag)	W4 (mag)	$E(K_s - W1)$ (mag)	$E(K_s - W2)$ (mag)	$E(K_s - W3)$ (mag)	$E(K_s - W4)$ (mag)
2	052638.83+065206.9	6.449 ± 0.079	6.435 ± 0.022	6.312 ± 0.016	4.766 ± 0.031	−0.019 ± 0.082	0.000 ± 0.032	0.132 ± 0.028	1.715 ± 0.039
4B	052840.51+011333.1	10.047 ± 0.023	9.879 ± 0.020	9.705 ± 0.042	8.370 ± 0.304	−0.031 ± 0.031	−0.003 ± 0.029	0.091 ± 0.047	1.286 ± 0.305
6	053115.70+053946.1	7.374 ± 0.035	7.405 ± 0.020	7.373 ± 0.018	6.606 ± 0.067	−0.019 ± 0.039	−0.055 ± 0.026	0.012 ± 0.025	0.694 ± 0.069
17A	052743.14+144611.7	8.899 ± 0.023	8.728 ± 0.021	8.604 ± 0.028	7.894 ± 0.216	0.037 ± 0.032	0.088 ± 0.030	0.132 ± 0.036	0.692 ± 0.217
27	052748.55+064545.6	9.306 ± 0.023	9.111 ± 0.020	8.918 ± 0.034	7.911 ± 0.238	−0.030 ± 0.030	0.005 ± 0.028	0.118 ± 0.039	0.995 ± 0.239
38	052430.10+064034.6	10.933 ± 0.023	10.684 ± 0.020	10.157 ± 0.072	8.390 ± 0.324	0.020 ± 0.032	0.019 ± 0.030	0.456 ± 0.075	2.123 ± 0.325
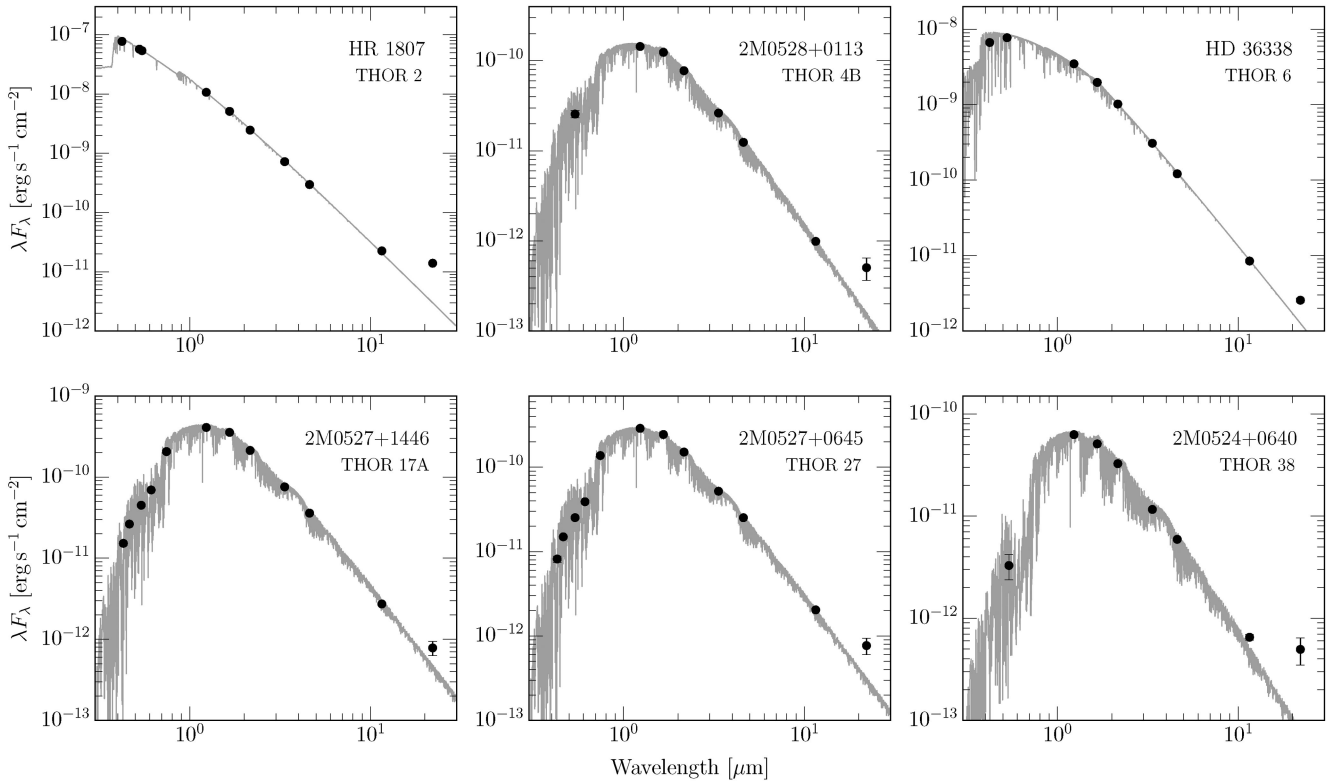
Figure 15. SEDs of six members of the 32 Ori group for which we have identified excess *W*4 emission at 22 μm. Note that the uncertainties on the individual points are typically smaller than the symbols used. In all cases except HR 1807, for which we used the ATLAS9 ODFNEW models, the BT-Settl CIFIST models have been adopted to compare against the photometric data.
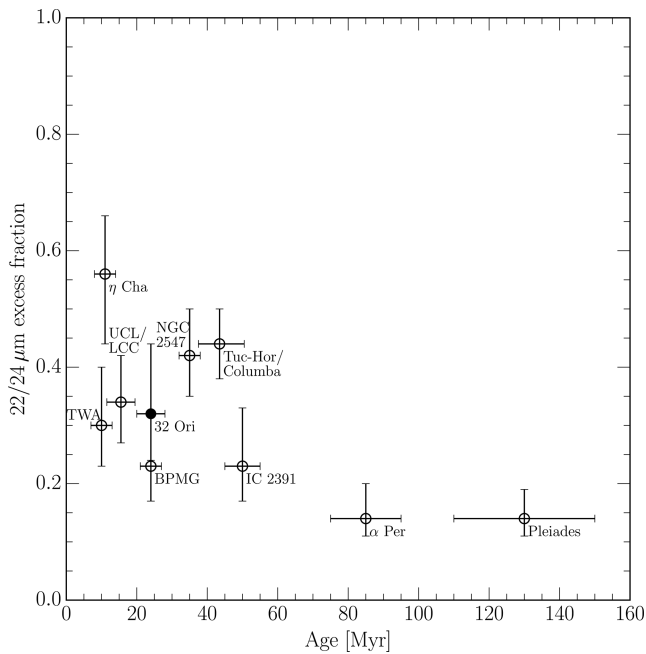

Figure 16. Debris disc fraction (as estimated from excess emission at either 22 or 24 μm) as a function of age for young nearby groups/associations and clusters. The disc fractions for all other regions have been taken from Zuckerman et al. (2012).

binomial statistics. The ages and uncertainties have been compiled from Barrado y Navascués, Stauffer & Jayawardhana (2004) for IC 2391, α Per and the Pleiades, Jeffries & Oliveira (2005) for NGC 2547, Bell et al. (2015) for TWA, η Cha, the BPMG and Tuc-Hor/Columba and Pecaut & Mamajek (2016) for UCL/LCC.

5.6 Spatial structure of the 32 ori group

Fig. 17 shows the *XYZ* spatial and *UVW* velocity distributions for the 45 stellar members of the 32 Ori group. Note that due to unreliable literature radial velocities for both HR 1807 and HD 35714, and missing radial velocities for HD 36823 and HD 36002 (SB2), these stars are not shown in the *UVW* panels of Fig. 17. From these distributions, we estimate a mean group position of $(X, Y, Z) = (-89.1 \pm 2.1, -26.0 \pm 1.3, -24.0 \pm 0.7)$ pc and velocity of $(U, V, W) = (-13.1 \pm 0.4, -18.9 \pm 0.2, -9.0 \pm 0.2)\,\mathrm{km\,s^{-1}}$, where the uncertainties on each represent the standard error of the mean. Due to the use of kinematic distances for the majority of the stars shown in Fig. 17, we would advise that, until additional *Gaia* parallaxes become available, the mean group *UVW* velocity listed in Table 2 be adopted for future searches for additional members.

Examining the *XYZ* distribution, we see that the geometry of the 32 Ori group is broadly ellipsoidal and elongated towards the Galactic Centre, with $(\Delta_X, \Delta_Y, \Delta_Z) \sim (60, 25, 20)$ pc. This is quite different from more filamentary/sheet-like geometries like those observed in TWA and Tuc-Hor (see Weinberger, Anglada-Escudé & Boss 2013; Kraus et al. 2014). Based on our derived age for the group, and assuming that all members formed within a region $\ll 1$ pc, the current dispersion in the *XYZ* plane suggests a one-dimensional internal velocity dispersion on the order of
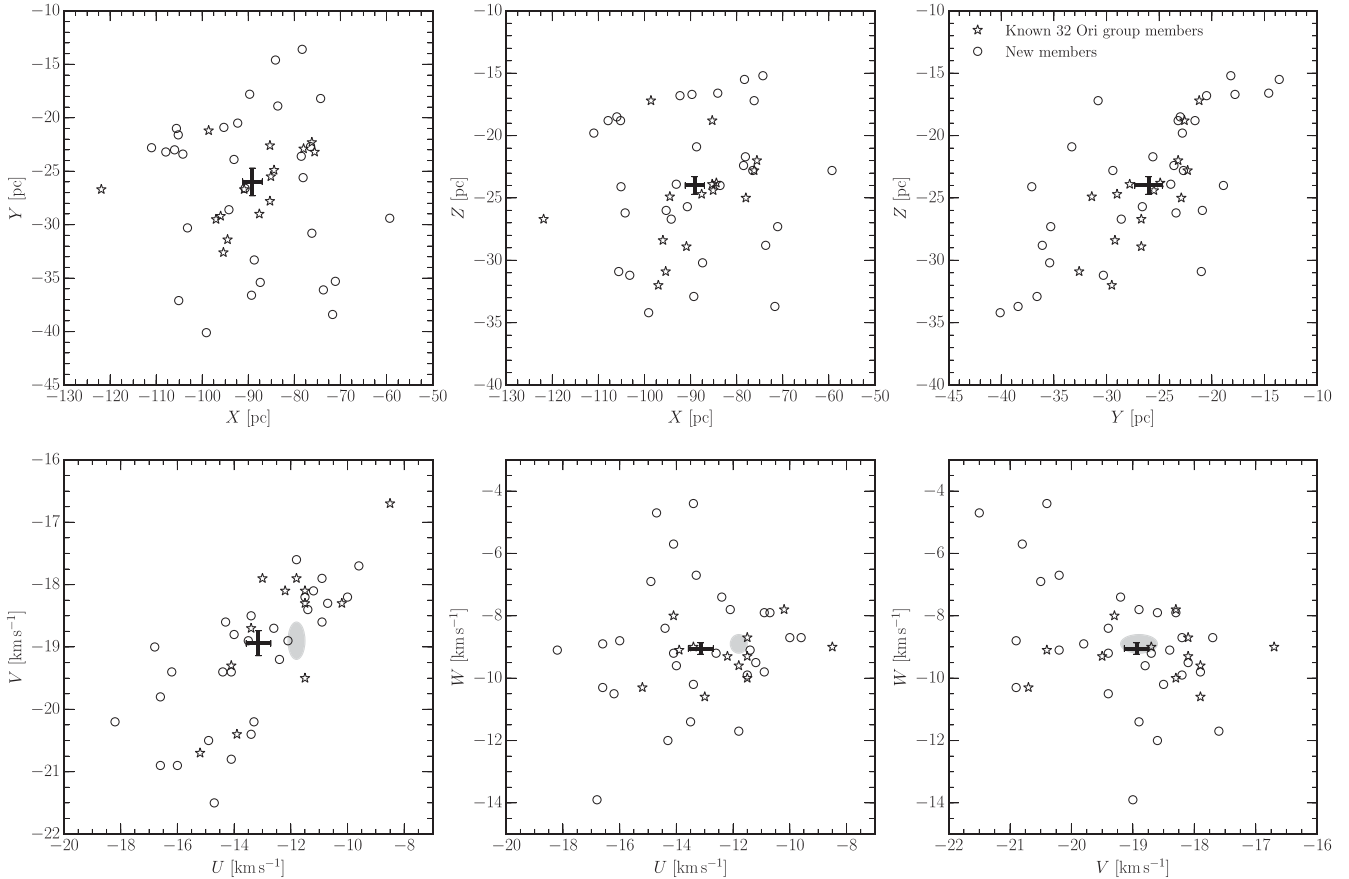
Figure 17. *XYZ* spatial (top row) and *UVW* velocity (bottom row) distribution for members of the 32 Ori group. Note that the known members HR 1807, HD 35714, HD 36823 and the new member HD 36002 are not included in the velocity plots because of unreliable or unavailable literature radial velocities. The black crosses represent the mean 32 Ori group space position and velocity of all members with the error bars corresponding to the standard error of the mean. The shaded region denotes the mean group *UVW* velocity as listed in Table 2.

1–$2\,\mathrm{km\,s^{-1}}$, which is consistent with those of other young moving groups and associations in the Local Bubble (Mamajek 2016). Furthermore, as argued by Kraus et al. (2014) for Tuc–Hor, the age of the 32 Ori group is much less than one Galactic orbital period and so we would not expect the tidal field of the Milky Way to have significantly influenced the current geometry of the group. Hence, the ellipsoidal shape more likely reflects the initial star formation conditions in which the group formed and could be more indicative of an originally compact cluster that has since become gravitationally unbound and is slowly dispersing into the Galactic field, as proposed for the ϵ Cha group (Murphy, Lawson & Bessell 2013).

6 CONCLUSIONS

We have undertaken the first large-scale systematic stellar census of the nearby but poorly studied 32 Orionis group. The main results from this study are as follows:

(i) Based on spectroscopic follow-up of candidate members selected from UCAC4 and URAT1, we have identified a total of 30 new members of the 32 Ori group; 29 M dwarf members and one A-type star that forms a comoving common proper motion pair with one of the new members. Members were confirmed by combining Li absorption, Hα emission and radial velocity information with kinematic distances and proper motions. This study has increased

the number of known group members by a factor of 3, bringing the total number of 32 Ori group members to 46.

(ii) We have unambiguously identified the Li depletion boundary (LDB) of the 32 Ori group. Using stellar evolutionary models, we derive ages from both isochronal fitting ($25 \pm 5\,\mathrm{Myr}$) and LDB analyses ($23 \pm 4\,\mathrm{Myr}$), which we combine to calculate a final adopted age for the 32 Ori group of $24 \pm 4\,\mathrm{Myr}$ ($\pm 4\,\mathrm{Myr}$ statistical, $\pm 2\,\mathrm{Myr}$ systematic). This age implies that the 32 Ori group is coeval with the somewhat closer β Pictoris moving group.

(iii) We have searched for the presence of circumstellar discs around the 45 stellar members of the 32 Ori group using the All*WISE* catalogue. As with other groups and associations of similar age, we find no evidence for prevailing warm, dusty discs; however, we have identified several possible debris discs based on excess emission in the *WISE W*4 band at 22 µm. From our limited sample of stars with *W*4 detections, we estimate a debris disc fraction of 32^{+12}_{-8} per cent for the group.

REFERENCES

Abt H. A., Morrell N. I., 1995, ApJS, 99, 135

Alcalá J. M. et al., 1996, A&AS, 119, 7

Alcalá J. M., Covino E., Torres G., Sterzik M. F., Pfeiffer M. J., Neuhäuser R., 2000, A&A, 353, 186

Allard F., Homeier D., Freytag B., 2011, in Johns-Krull C., Browning M. K., West A. A., eds, ASP Conf. Ser. Vol. 448, 16th Cambridge Workshop on Cool Stars, Stellar Systems, and the Sun. Astron. Soc. Pac., San Francisco, p. 91

Baraffe I., Homeier D., Allard F., Chabrier G., 2015, A&A, 577, 42

Barbier-Brossat M., Figon P., 2000, A&AS, 142, 217

Barrado y Navascués D., Stauffer J. R., Jayawardhana R., 2004, ApJ, 614, 386

Bayo A., Rodrigo C., Barrado y Navascués D., Solano E., Gutiérrez R., Morales-Calderón M., Allard F., 2008, A&A, 492, 277

Bell C. P. M., Naylor T., Mayne N. J., Jeffries R. D., Littlefair S. P., 2013, MNRAS, 434, 806

Bell C. P. M., Rees J. M., Naylor T., Mayne N. J., Jeffries R. D., Mamajek E. E., Rowe J., 2014, MNRAS, 445, 3496

Bell C. P. M., Mamajek E. E., Naylor T., 2015, MNRAS, 454, 593

Bessell M. S., 1999, PASP, 111, 1426

Bhatt N. H., Cami J., 2015, ApJS, 216, 22

Bilir S., Ak S., Karaali S., Cabrera-Lavers A., Chonis T. S., Gaskell C. M., 2008, MNRAS, 384, 1178

Binks A. S., Jeffries R. D., 2014, MNRAS, 438, L11

Binks A. S., Jeffries R. D., 2016a, MNRAS, preprint (arXiv:1611.07416)

Binks A. S., Jeffries R. D., 2016b, MNRAS, 455, 3345

Bobylev V. V., Goncharov G. A., Bajkova A. T., 2006, Astron. Rep., 50, 733

Bochanski J. J., West A. A., Hawley S. L., Covey K. R., 2007, AJ, 133, 531

Bouy H., Alves J., 2015, A&A, 584, A26

Bressan A., Marigo P., Girardi L., Salasnich B., Dal Cero C., Rubele S., Nanni A., 2012, MNRAS, 427, 127

Burgasser A. J. et al., 2016, ApJ, 820, 32

Caffau E., Ludwig H. G., Steffen M., Freytag B., Bonifacio P., 2011, Sol. Phys., 268, 255

Cameron E., 2011, PASA, 28, 128

Canup R. M., 2004, ARA&A, 42, 441

Cardelli J. A., Clayton G. C., Mathis J. S., 1989, ApJ, 345, 245

Castelli F., Kurucz R. L., 2004, in Piskunov N. E., Weiss W. W., Gray D. F., eds, Proc. IAU Symp. 210, Modelling of Stellar Atmospheres. Astron. Soc. Pac., San Francisco, p. 20

Choquet É. et al., 2016, ApJ, 817, L2

Cutri R. M. et al., 2003, 2MASS Point Source Catalogue, available at http://www.ipac.caltech.edu/2mass/

Cutri R. M. et al., 2014, VizieR Online Data Catalog, 2328

da Silva L., Torres C. A. O., de La Reza R., Quast G. R., Melo C. H. F., Sterzik M. F., 2009, A&A, 508, 833

de la Reza R., Torres C. A. O., Quast G., Castilho B. V., Vieira G. L., 1989, ApJ, 343, L61

Dias W. S., Alessi B. S., Moitinho A., Lépine J. R. D., 2002, A&A, 389, 871

Dias W. S., Monteiro H., Caetano T. C., Lépine J. R. D., Assafin M., Oliveira A. F., 2014, A&A, 564, 79

Dolan C. J., Mathieu R. D., 2002, AJ, 123, 387

Dopita M., Hart J., McGregor P., Oates P., Bloxham G., Jones D., 2007, Ap&SS, 310, 255

Dotter A., Chaboyer B., Jevremović D., Kostov V., Baron E., Ferguson J. W., 2008, ApJS, 178, 89

Drake A. J. et al., 2013, ApJ, 763, 32

Drake A. J. et al., 2014, ApJS, 213, 9

Ducourant C., Teixeira R., Périé J. P., Lecampion J. F., Guibert J., Sartori M. J., 2005, A&A, 438, 769

Duerr R., Imhoff C. L., Lada C. J., 1982, ApJ, 261, 135

Edwards T. W., 1976, AJ, 81, 245

Elliott P., Bayo A., Melo C. H. F., Torres C. A. O., Sterzik M., Quast G. R., 2014, A&A, 568, 26

Feiden G. A., Chaboyer B., 2013, ApJ, 779, 183

Feiden G. A., Chaboyer B., 2014, ApJ, 789, 53

Franciosini E., Sacco G. G., 2011, A&A, 530, 150

Friedemann C., 1992, Bull. Inf. Cent. Donnees Stellaires, 40, 31

Fuhrmeister B., Schmitt J. H. M. M., 2004, A&A, 420, 1079

Gagné J., Lafrenière D., Doyon R., Malo L., Artigau É., 2014, ApJ, 783, 121

Gaia Collaboration et al., 2016, A&A, 595, 2

Gizis J. E., Reid I. N., Hawley S. L., 2002, AJ, 123, 3356

Gontcharov G. A., 2006, Astron. Lett., 32, 759

Gregorio-Hetem J., Lepine J. R. D., Quast G. R., Torres C. A. O., de La Reza R., 1992, AJ, 103, 549

Guenther E. W., Emerson J. P., 1997, A&A, 321, 803

Hauck B., Mermilliod M., 1998, A&AS, 129, 431

Henden A. A., Levine S. E., Terrell D., Smith T. C., Welch D., 2012, J. Am. Assoc. Var. Star Obs., 40, 430

Henden A. A., Templeton M., Terrell D., Smith T. C., Levine S., Welch D., 2016, VizieR Online Data Catalog, 2336

Hohle M. M., Neuhäuser R., Schutz B. F., 2010, Astron. Nachr., 331, 349

Houdebine E. R., Foing B. H., Rodono M., 1990, A&A, 238, 249

Janson M., Bonavita M., Klahr H., Lafrenière D., Jayawardhana R., Zinnecker H., 2011, ApJ, 736, 89

Jeffries R. D., 2006, in Randich S., Pasquini L., eds, Chemical Abundances and Mixing in Stars in the Milky Way and its Satellites. Springer, p. 163

Jeffries R. D., Oliveira J. M., 2005, MNRAS, 358, 13

Jeffries R. D., Naylor T., Mayne N. J., Bell C. P. M., Littlefair S. P., 2013, MNRAS, 434, 2438

Johnson H. L., 1966, ARA&A, 4, 193

Kharchenko N. V., Piskunov A. E., Schilbach E., Röser S., Scholz R. D., 2013, A&A, 558, 53

Kraus A. L., Shkolnik E. L., Allers K. N., Liu M. C., 2014, AJ, 147, 146

Lagrange A. M. et al., 2010, Science, 329, 57

Lestrade J. F., Wyatt M. C., Bertoldi F., Menten K. M., Labaigt G., 2009, A&A, 506, 1455

Luhman K. L., Mamajek E. E., 2012, ApJ, 758, 31

Mace G. N., Prato L., Wasserman L. H., Schaefer G. H., Franz O. G., Simon M., 2009, AJ, 137, 3487

Malo L., Doyon R., Lafrenière D., Artigau É., Gagné J., Baron F., Riedel A., 2013, ApJ, 762, 88

Malo L., Doyon R., Feiden G. A., Albert L., Lafrenière D., Artigau É., Gagné J., Riedel A., 2014, ApJ, 792, 37

Mamajek E. E., 2007, in B.G. Elmegreen, J. Palous, eds, Proc. IAU Symp. 237, Triggered Star Formation in a Turbulent ISM. Cambridge Univ. Press, p. 442

Mamajek E. E., 2016, in Kastner J. H., Stelzer B., Metchev S. A., eds, Proc. IAU Symp. 314, Young Stars and Planets Near the Sun. Cambridge Univ. Press, p. 21

Mamajek E. E., Bell C. P. M., 2014, MNRAS, 445, 2169

Mamajek E. E., Meyer M. R., Liebert J., 2006, AJ, 131, 2360

Melis C., Zuckerman B., Rhee J. H., Song I., Murphy S. J., Bessell M. S., 2012, Nature, 487, 74

Melis C., Reid M. J., Mioduszewski A. J., Stauffer J. R., Bower G. C., 2014, Science, 345, 1029

Mentuch E., Brandeker A., van Kerkwijk M. H., Jayawardhana R., Hauschildt P. H., 2008, ApJ, 689, 1127

Mermilliod J. C., 2006, VizieR Online Data Catalog, 2168

Metchev S. A., Hillenbrand L. A., 2009, ApJS, 181, 62

Murphy S. J., Lawson W. A., 2015, MNRAS, 447, 1267

Murphy S. J., Lawson W. A., Bessell M. S., 2013, MNRAS, 435, 1325

Naylor T., 2009, MNRAS, 399, 432

Naylor T., Jeffries R. D., 2006, MNRAS, 373, 1251

Nidever D. L., Marcy G. W., Butler R. P., Fischer D. A., Vogt S. S., 2002, ApJS, 141, 503

Palla F., Randich S., Pavlenko Y. V., Flaccomio E., Pallavicini R., 2007, ApJ, 659, L41

Pecaut M. J., Mamajek E. E., 2013, ApJS, 208, 9

Pecaut M. J., Mamajek E. E., 2016, MNRAS, 461, 794

Pickles A. J., 1998, PASP, 110, 863

Reis W., Corradi W., de Avillez M. A., Santos F. P., 2011, ApJ, 734, 8

Riedel A. R., Alam M. K., Rice E. L., Cruz K. L., Henry T. J., 2016, ApJ, preprint (arXiv:1610.03867)

Röser S., Demleitner M., Schilbach E., 2010, AJ, 139, 2440

Rucinski S. M., Krautter J., 1983, A&A, 121, 217

Shaya E. J., Olling R. P., 2011, ApJS, 192, 2

Shvonski A. J., Mamajek E. E., Meyer M. R., Kim J. S., 2010, BAAS, 42, 428.22

Shvonski A. J., Mamajek E. E., Kim J. S., Meyer M. R., Pecaut M. J., 2016, preprint (arXiv:1612.06924)

Silverberg S. M. et al., 2016, ApJ, 830, L28

Soderblom D. R., Jones B. F., Balachandran S., Stauffer J. R., Duncan D. K., Fedele S. B., Hudon J. D., 1993, AJ, 106, 1059

Soderblom D. R., Hillenbrand L. A., Jeffries R. D., Mamajek E. E., Naylor T., 2014, in Beuther H., Klessn R. S., Dullemond C. P., Henning T. K., eds, Protostars and Planets VI. Univ. Arizona Press, p. 219

Stauffer J. R., Schild R., Barrado y Navascues D., Backman D. E., Angelova A. M., Kirkpatrick J. D., Hambly N., Vanzi L., 1998, ApJ, 504, 805

Stauffer J. R. et al., 2007, ApJS, 172, 663

Taylor M. B., 2005, in Shopbell P., Britton M., Ebert R., eds, ASP Conf. Ser. Vol. 347, Astronomical Data Analysis Software and Systems XIV. Astron. Soc. Pac., San Francisco, p. 29

Tognelli E., Prada Moroni P. G., Degl'Innocenti S., 2015, MNRAS, 449, 3741

Tonry J., Davis M., 1979, AJ, 84, 1511

Torres C. A. O., da Silva L., Quast G. R., de la Reza R., Jilinski E., 2000, AJ, 120, 1410

Torres C. A. O., Quast G. R., Melo C. H. F., Sterzik M. F., 2008, in Reipurth B., ed., Handbook of Star Forming Regions Vol. II, The Southern Sky. Astron. Soc. Pac., San Francisco, p. 757

van Leeuwen F., 2007, A&A, 474, 653

Voges W. et al., 1999, A&A, 349, 389

Webb R. A., Zuckerman B., Platais I., Patience J., White R. J., Schwartz M. J., McCarthy C., 1999, ApJ, 512, L63

Weinberger A. J., Anglada-Escudé G., Boss A. P., 2013, ApJ, 762, 118

West A. A. et al., 2011, AJ, 141, 97

White R. J., Gabor J. M., Hillenbrand L. A., 2007, AJ, 133, 2524

Zacharias N., Monet D. G., Levine S. E., Urban S. E., Gaume R., Wycoff G. L., 2005, VizieR Online Data Catalog, 1297

Zacharias N., Finch C. T., Girard T. M., Henden A., Bartlett J. L., Monet D. G., Zacharias M. I., 2013, AJ, 145, 44

Zacharias N. et al., 2015, AJ, 150, 101

Zorec J., Cidale L., Arias M. L., Frémat Y., Muratore M. F., Torres A. F., Martayan C., 2009, A&A, 501, 297

Zuckerman B., Song I., 2004, ARA&A, 42, 685

Zuckerman B., Webb R. A., 2000, ApJ, 535, 959

Zuckerman B., Melis C., Rhee J. H., Schneider A., Song I., 2012, ApJ, 752, 58

SUPPORTING INFORMATION

Supplementary data are available at *MNRAS* online.

Table 3. Spectroscopic parameters and membership assignments for the candidate members and 11 known members of the 32 Ori group observed with WiFeS.

Please note: Oxford University Press is not responsible for the content or functionality of any supporting materials supplied by the authors. Any queries (other than missing material) should be directed to the corresponding author for the article.

This paper has been typeset from a TEX/LATEX file prepared by the author.